INSTITUTO DE FÍSICA

Universidade Federal Fluminense

# A Study of Strangelets in Astrophysical Environments

Doctoral Thesis

Jonathan Joás Zapata Campos

jonathanzapata@id.uff.br

Institute of Physics
Universidade Federal FLuminense
Niterói-RJ

**Supervisors:**
Prof. Dr. Rodrigo Negreiros

August 5, 2022

Ficha catalográfica automática - SDC/BIF
Gerada com informações fornecidas pelo autor

Z35s Zapata campos, Jonathan Joás
A Study of Strangelets in Astrophysical Environments / Jonathan Joás Zapata campos ; Rodrigo Picanço Negreiros, orientador. Niterói, 2022.
99 f. : il.

Tese (doutorado)-Universidade Federal Fluminense, Niterói, 2022.

DOI: http://dx.doi.org/10.22409/PPGF.2022.d.06366795789

1. Strange quark matter. 2. Strangelets. 3. Planets. 4. Quark stars. 5. Produção intelectual. I. Picanço Negreiros, Rodrigo, orientador. II. Universidade Federal Fluminense. Instituto de Física. III. Título.

CDD -

Bibliotecário responsável: Debora do Nascimento - CRB7/6368

**JONATHAN JOÁS ZAPATA CAMPOS**

# A STUDY OF STRANGELETS IN ASTROPHYSICAL ENVIRONMENTS

Doctoral thesis presented to the Postgraduate Program of the Institute of Physics of the Universidade Federal Fluminense as a partial requirement for obtaining a Doctor's Degree in Physics. Area of concentration: Astrophysics.

**Supervisor:**

PROF. DR. RODRIGO NEGREIROS

Niterói
2022

JONATHAN JOÁS ZAPATA CAMPOS

# A STUDY OF STRANGELETS IN ASTROPHYSICAL ENVIRONMENTS

Doctoral thesis presented to the Postgraduate Program of the Institute of Physics of the Universidade Federal Fluminense as a partial requirement for obtaining a Doctor's Degree in Physics. Area of concentration: Astrophysics.

**Dissertation Committee:**

---

Dr. Rodrigo Picanço Negreiros
(supervisor)
IF-UFF

---

Dr. Mariana Dutra da Rosa Lourenço
ITA

---

Dr. Raissa Fernandes Pessoa Mendes
IF-UFF

---

Dr. Ricardo Luciano Sonego Farias
UFSM

---

Dr. Sergio Jose Barbosa Duarte
CBPF

# Acknowledgements

First, I thank *YHVH* for the opportunity to study in this pleasant country, Brazil, which I call my second home, and also, I thank the people who were with me and who in some other way helped me in my professional training. I would like to list some of them: grateful for my Peruvian parents, grateful for my American parents, grateful for my friends from church and college, grateful for my professors at UFF who willingly taught us, grateful for my advisor Rodrigo Picanço N. and his patience throughout my academic training. Furthermore, I am very grateful to the *Coordenação de Aperfeiçoamento de Pessoal de Nível Superior* (CAPES) and the *Conselho Nacional de Desenvolvimento Científico e Tecnológico* (CNPq) for their financial support throughout my academic career here in Brazil.

# Abstract

In this thesis, we will explore the manifestation of strange quark matter in astrophysical environments, particularly in the context of compact objects, and planets-like objects. We consider the "strange quark matter hypothesis", that is, matter consisting of a combination of up, down, and strange quarks could be absolutely stable. Small nuggets of such matter are called "strangelets" and large pieces (kilometer-sized) are "strange stars". In this context, first, we consider the possibility that strange quark matter may manifest itself in the form of planet-like objects made of strangelets organized in a crystalline structure. These objects we call strangelet crystal planets. We also calculate the relevant quantities that could potentially be observable, such as the planetary tidal disruption radius and the gravitational wave signals that may arise from potential star-planet merger events. Thus, we find that strangelet crystal planet have masses that are similar to ordinary planets, but slightly smaller radii. Additionally, they display intermediate behavior with possible orbital properties not as extreme as those of strange planets (composed of strange quark matter in a gaseous-like state, i.e. not clumped in nuggets) but not as mild as those of ordinary planets. The second part of this thesis is dedicated to the study of quark stars. In this case, these objects are composed of quark matter core crusted by strangelets. Our main purpose is to quantify the effects of strangelets crust matter on the thermal properties and relaxation times of those quark stars. We also consider the possibility color superconductivity effects in the quark core. In this way, we have found that quark stars with strangelet crusts (thinner crusts) display a faster cooling behavior when compared with quark stars with nuclear crusts (thicker crusts). We will show that quark stars with strangelet crusts have a significantly thermal relaxation time different from those with nuclear matter crusts. The studies carried out in this thesis approach strangelet manifestations in compact objects, and it provides some effective methods to test the strange quark matter hypothesis.

**Keywords**: quark matter, strangelets, planets, quark stars.

# Resumo

Nesta tese, exploraremos a manifestação da matéria de quarks estranha em ambientes astrofísicos, particularmente no contexto de objetos compactos e objetos semelhantes a planetas. Levamos em conta a "hipótese da matéria de quarks estranha", ou seja, a matéria consistindo de uma combinação de quarks up, down e strange poderia ser absolutamente estável. Pequenas pepitas de tal matéria são chamadas "strangelets" e pedaços grandes (do tamanho de quilômetros) são "estrelas estranhas". Neste contexto, primeiro, consideramos a possibilidade de que a matéria de quarks estranha possa se manifestar na forma de objetos semelhantes aos planetas feitos de strangelets organizados em uma estrutura cristalina. Esses objetos nós chamamos planetas cristalinos de strangelets. Também calculamos as quantidades relevantes que poderiam ser potencialmente observáveis, como o raio de ruptura das marés planetárias e os sinais de ondas gravitacionais que podem surgir de potenciais eventos de fusão estrela-planeta. Desta forma, descobrimos que os planetas cristalinos de strangelets têm massas semelhantes aos planetas comuns, mas raios ligeiramente menores. Além disso, eles exibem um comportamento intermediário com possíveis propriedades orbitais não tão extremas quanto as de planetas estranhos (compostos de matéria de quarks estranha em estado gasoso, ou seja, não aglomerados em pepitas), mas não tão moderadas quanto as de planetas comuns. A segunda parte desta tese é dedicada ao estudo das estrelas de quarks. Nesse caso, esses objetos são compostos de núcleo de matéria quarks com crostas de strangelets. Nosso principal objetivo é quantificar os efeitos da matéria da crosta de strangelets nas propriedades térmicas e nos tempos de relaxamento dessas estrelas. Incluímos, também, os possíveis efeitos de supercondutividade de cor no núcleo de quarks. Desta forma, descobrimos que estrelas de quarks com crostas de strangelets (crostas mais finas) apresentam um comportamento de resfriamento mais rápido quando comparadas com estrelas de quarks com crostas nucleares (crostas mais grossas). Além disso, mostraremos que estrelas de quarks com crostas de strangelets têm um tempo de relaxamento térmico significativamente diferente daquelas com crostas de matéria nuclear. Os estudos realizados nesta tese abordam manifestações de strangelets em objetos compactos e fornecem alguns métodos eficazes para testar a hipótese de matéria de quarks estranha.

**Palavras-chave**: matéria estranha, strangelets, planetas, estrela de quarks.

# List of Figures

# List of Tables

# Contents

Chapter 1

# Introduction

In astrophysics we employ methods and principles of physics and mathematics to study astronomical objects and their properties. Some topics of study by astrophysicists include solar systems, extrasolar planets, stellar dynamics and structure, and compact objects. Astrophysicists distinguish three types of compact objects: white dwarfs (WD), neutron stars (NS) and black holes (BH). In particular, neutron stars are residues of massive stars that eject matter in the process known as a supernova explosion (Weber, 2017; Glendenning, 2012). Neutron stars have typical masses of $\sim 1.4M$ (solar masses[1]) and radii about 10 km. This makes them have core densities that can be ten times ($\sim 10^{15}\ g/cm^3$) greater than the nuclear saturation density[2]. Also, there is an expectation that at such extreme densities, new states of matter will be produced. One such intriguing possibility is that compact stars consist of strange quark matter made up of *up*, *down*, and *strange* quarks, which could be more stable than ordinary nuclear matter and all atomic nuclei (Weber, 2017). This is known as strange quark matter (SQM) hypothesis. However, the internal composition of these compact objects is still largely studied.

It has been suggested that strange quark matter state may exist in the core due to the high density at the center (several times of nuclear saturation density) (Bodmer, 1971; Witten, 1984; Farhi and Jaffe, 1984). Taking into account the SQM hypothesis, the existence of a whole sequence of strange quark matter (SQM) objects, such as strange quark stars (Witten, 1984; Farhi and Jaffe, 1984; Alcock et al., 1986), strange quark dwarfs (Glendenning et al., 1995), and strange quark planets (Glendenning et al., 1995; Horvath, 2012; Huang and Yu, 2017) were proposed. Even in Glendenning et al. (1995), SQM objects may be

[1] See Physical Constant in Appendix A

[2] Nuclear saturation density is $2.8 \times 10^{14}\ g/cm^3$

covered by a thin crust of normal hadronic matter, or may simply be bare SQM cores. However, the common compact nature of strange stars and neutron stars makes it difficult to discriminate them by current astronomical observations (Alcock et al., 1986). To get around this issue, some works were made to reveal the difference between them, for example, they may have different mass–radius relations (Witten, 1984; Glendenning et al., 1995), different rotation periods (Friedman et al., 1989; Frieman and Olinto, 1989; Madsen, 1998), different cooling rate (Pizzochero, 1991; Page and Applegate, 1992; Ma et al., 2002), different gravitational wave features (Madsen, 1998; Jaranowski et al., 1998; Geng et al., 2015), different maximum masses (Lai and Xu, 2009; Li et al., 2010; Shibata et al., 2019), and so on. Nevertheless, the problem still remains unsolved. Taking this in mind, in this thesis, we pretend to approach this problem and give an alternative to test SQM hypothesis in the context of planets-like objects and compact objects.

The hypothesis of strange quark matter (SQM), i.e. matter consisting of up, down, and strange quarks is absolutely stabler than hadronic matter has been proposed by Bodmer (1971); Witten (1984); Terazawa (1979). In recent years, many authors investigated how such matter would manifest in nature, see for instance Madsen (1999); Weber (2005); Buballa (2005); Kurkela et al. (2010). Possibilities included little quark lumps called strangelets[3] (a few Fermi) and large compact stars ($\sim km$) made entirely of strange quark matter (Alcock et al., 1986; Baym and Chin, 1976; Haensel et al., 1986b,a). Particularly, the authors Farhi and Jaffe (1984) and Berger and Jaffe (1987) calculated a mass formula for strangelets, later this approach has been improved by Heiselberg (1993); Heiselberg et al. (1993) and he found a more accurate mass formula considering the charge distribution that vary on the scale of the Debye screening length. Furthermore, in Witten (1984); Alcock et al. (1986); Glendenning et al. (1995); Haensel et al. (1986b,a); Kettner et al. (1995), the authors developed the concept of strange quark stars, that is, objects consisting of strange matter cores surrounded by nuclear crusts. They found a complete sequence of strange stars that range from very compact members, with properties similar to those of neutron stars to white dwarf-like objects, to planetary-like strange matter objects. It was pointed out that the minimum-mass configuration in such sequence is $0.017M$ (Glendenning et al., 1995; Kettner et al., 1995). On top of that, Alford

[3]The term *strangelet* is a hyperdiminutive of the English word "*strange*"

et al. (2012) investigated dwarf-like objects that consist of a crystal of positively charged strangelets in a neutralizing background of electrons, they named these objects as *strangelet dwarfs*.

Encouraged by the works previously exposed above, we especially focused our research on the following works: Alford et al. (2012) who performed a study on strangelet dwarfs, which consist of a crystalline structure of strangelets in a sea of electrons as well Heiselberg's mass formula for strangelets (Heiselberg, 1993) however, we center of attention in planet-like objects. Also, Alcock et al. (1986), in which they considered the possibility for a strange star to maintain a crust of normal matter, and Jaikumar et al. (2006) which considered the possibility of a crust of strangelets embedded in a uniform electron background on the surface of strange stars. In the work presented here, we follow Alcock et al. (1986); Alford et al. (2012); Jaikumar et al. (2006) except, we center on planetary-like objects, characterized by low pressure and, quark stars crusted by strangelets (Jaikumar et al., 2006). Along these lines, to planetary-like objects proposed here, we study their properties such as mass, radii, and possible orbital properties, on the other hand, as to quark stars, we will explore the effects of strangelets crust on the cooling analysis and the thermal relaxation of these quark stars. Our work is the first in this type of analysis.

Therefore, our contribution is to provide a possible manifestation of strangelets and how we could identify SQM objects. Thus, we present an alternative of planet-like objects called strangelet crystal planets and study their main properties (Zapata and Negreiros, 2020). Similarly, explore strange stars with strangelet crusts and quantify their thermal properties (Zapata, J. et al., 2022). We base our thesis on the theoretical hypothesis of strange quark matter. Phenomenologically speaking, the connection between theses two objects studied in this research is the behavior of strange quark matter at different densities. As in Glendenning et al. (1995) where the authors determined all possible equilibrium sequences of compact strange-matter stars with nuclear crusts, which range from massive strange stars to strange white-dwarf-like objects (strange dwarfs), we argue a possible sequence of compact objects that consist a core of strange matter enveloped within strangelet crystal planets matter. Specially, we focus on planetary-like objects and quark stars with strangelets crust.

This thesis is organized as follows: in chapter 2 we begin to study the foundations of this thesis, that is, the strange quark matter hypothesis, the strangelets and their mass formula, the possibility to have strangelet crusts on quark stars' surfaces, and ends with the equation of state of strange quark matter. With the foundations in place, in chapter 3 we will explore the possible existence of strangelet crystal planets as well discuss their orbital properties. Afterward, in Chap. 4 we will examine the cooling and the thermal relaxation of isolated quark stars crusted by strangelet. We also analyzed quark stars crusted by ordinary nuclear matter for comparison purposes. Finally, in Chap. 5 we will present our conclusions and suggest possible future studies to be based on this research.

Chapter 2

# Strange Quarks Matter

## 2.1 Introduction

It is well known that hadrons (protons and neutrons) are composed of a substructure of particles called quarks. In fact, all hadrons can be understood as a composition of quarks, three of which are needed to form baryons (for example, the neutron is formed by the combination of one up and two down quarks). Quarks are found in six flavors: up (u), down (d), strange (s), charm (c), top (t) and bottom (b). Currently, quarks, along with leptons and bosons, are thought of as fundamental or elementary particles.

In the astrophysical context, there are three categories of compact objects: white dwarfs (WD), neutron stars (NS), and black holes (BH). White dwarfs are theoretically formed from small and medium-mass stars (less than $\sim 8M_\odot$). A typical WD is approximately as massive as the sun, yet only slightly larger than Earth. This makes white dwarfs contain one of the densest forms of matter ($\sim 10^9\ g/cm^3$). As for black holes, they constitute a region of space-time with such a concentration of matter and energy that no particle (not even light) inside the black hole can escape its gravitational force. Finally, neutron stars, which are residues of massive stars (with masses greater than $8M_\odot$) that eject matter in the supernova explosion process. Neutron stars have a radius on the order of 10 km and a mass of about $1.4M_\odot$. It makes neutron stars, the smallest and densest currently known class of stellar objects (Glendenning, 2012). However, according to model calculations, neutron stars are far from being composed of only neutrons but may contain a large fraction of strangeness[1]–carrying hyperons

[1]Strangeness is a property of particles expressed as a quantum number, for describing decay of particles in strong and electromagnetic interactions which occur in a short period of time.

which are possible in phase equilibrium with u, d, s–quark matter (Weber, 2017). Nevertheless, if the cores of neutron star have high compressed matter, then neutrons inside the star transforms into its deconfined phase, quark matter. Indeed, there is the possibility that that ground state may be strange quark matter, made up of u, d, s quarks, instead of iron. If it is possible, then it appears likely that all neutron stars would have to be strange quark matter stars (Weber, 2017; Madsen, 1998). Quark stars are composed of quark matter. Such a state of matter was conceived of soon after the realization that quarks, the constituents of nucleons, are asymptotically free. At the extreme of asymptotic momentum transfer, density, or temperature, quark are free of interaction. Under these circumstances, the individuality of nucleons is lost, and the quarks of nuclear matter are free to explore a much larger "colorless" region of space referred to as quark matter.

Hence, in this chapter we present the main basis of our work that will be used to develop this thesis, that is, the strange quark matter hypothesis, the strangelets and their mass formula, the possibility of crystal structures made of strangelets on the surfaces of quark stars, and the equation of state (EOS) for strange quark matter.

## 2.2 Strange Quark Matter Hypothesis

Firstly, we consider the theoretical strange quark matter (SQM) hypothesis as proposed by Bodmer (1971); Witten (1984) and Terazawa (1979). According to this hypothesis, the true and absolute ground state of the strong interactions is the deconfined state of quark matter consisting of an approximately equal proportion of *up*, *down* and *strange* quarks. That is, strange matter may have an energy per baryon that is less than that of nuclear matter. This is called *strange quark matter*. In the following, we describe the possible absolute stability of strange quark matter.

Experimentally, no quarks have been isolated, this leads to the concept that quarks are characterized by their confinement inside the hadrons. A useful phenomenological description of quarks in hadrons is provided by the MIT[2] bag model. For this model, the pressure $P^f$ of the individual quarks and leptons contained in the bag is counterbalanced by the total external pressure in the

[2]MIT stands for Massachusetts Institute of Technology.

bag, $P + B$, according to

$$P + B = \sum_f P^f, \tag{2.1}$$

while the energy density of the quarks confined in the bag is given by

$$\epsilon = \sum_f \epsilon^f + B. \tag{2.2}$$

where $\epsilon^f$ are the contributions of the individual quarks to the total energy density and, the quantity $B$ denotes the bag constant[3]. The contributions of each quark flavor to pressure, energy density, and baryonic number density are determined by the thermodynamic potentials, from which one obtains

$$P^f = \frac{\gamma_f}{6\pi^2} \int_0^{k_{F_f}} dk \frac{k^4}{\sqrt{k^2 + m_f^2}}, \tag{2.3}$$

$$\epsilon^f = \frac{\gamma_f}{2\pi^2} \int_0^{k_{F_f}} dk k^2 \sqrt{k^2 + m_f^2}, \tag{2.4}$$

$$\rho^f = \frac{\gamma_f}{6\pi^2} k_{F_f}^3. \tag{2.5}$$

The quantity $\mu^f$ denotes the chemical potential of the flavor quark $f$, and $m_f$ represents its mass. The phase space factor $\gamma_f = 2(spin) \times 3(color) = 6$.

Let us consider massless quarks inside a confining bag at zero temperature. For a massless quark flavor, $f$, the Fermi momentum, $k_{F_f}$, equals the chemical potential, $\mu^f$ ($\mu = \sqrt{k^2 + m^2}$). The number densities are therefore given by

$$\rho^f = \frac{(\mu^f)^3}{\pi^2}, \tag{2.6}$$

the energy densities by

$$\epsilon^f = 3\frac{(\mu^f)^4}{4\pi^2}, \tag{2.7}$$

and, the pressures given by

$$P^f = \frac{(\mu^f)^4}{4\pi^2} = \frac{\epsilon^f}{3}. \tag{2.8}$$

At zero external bag pressure, the sum of the quark pressures is balanced by the

[3]In fact, $B$ is the energy cost per unit volume to keep the quarks in the bag.

confining bag pressure, $B$, i.e.

$$\Sigma_f P^f = B. \tag{2.9}$$

This gives for the total energy density inside the bag

$$\epsilon = \Sigma_f \epsilon^f + B. \tag{2.10}$$

The total baryon number density is

$$\rho = \Sigma_f \rho^f / 3. \tag{2.11}$$

For a gas of massless $u$ (charge $+\frac{2}{3}e$) and $d$ (charge $-\frac{1}{3}e$) quarks electric charge neutrality,

$$\frac{2}{3}\rho^u - \frac{1}{3}\rho^d = 0, \tag{2.12}$$

requires that $\rho^d = 2\rho^u$, or $\mu_2 \equiv \mu^u = \mu^d/2^{1/3}$. The corresponding 2-flavor quark pressure then follows as

$$P_2 \equiv P^u + P^d = \left(1 + 2^{4/3}\right) \frac{\mu_2^4}{4\pi^2} = B. \tag{2.13}$$

From the total energy density, $\epsilon_2 = 3P_2 + B = 4B$, and the baryon number density,

$$\rho_2 = \frac{\rho^u + \rho^d}{3} = \frac{\mu_2^3}{\pi^2}, \tag{2.14}$$

one obtains for the energy per baryon of 2-flavor quark matter,

$$\left(\frac{E}{A}\right)_2 \equiv \frac{\epsilon_2}{\rho_2} = \frac{4B}{\rho_2} = 934 MeV \times B_{145}^{1/4}, \tag{2.15}$$

where $B_{145}^{1/4} \equiv B^{1/4}/145$ MeV. A value of 145 MeV is the lowest possible choice for $B^{1/4}$ (Weber, 2017).

On the other hand, a 3-flavor quark gas is electrically neutral for[4],

$$\rho^u = \rho^d = \rho^s, \tag{2.16}$$

that is, $\mu_3 \equiv \mu^u = \mu^d = \mu^s$. For fixed bag constant, the 3-flavor quark gas should exert the same pressure as the 2-flavor gas, i.e., $P_3 = P_2$. This implies for the

[4] strange quark (charge $-\frac{1}{3}e$)

chemical potentials

$$\mu_3 = \left[\frac{(1+2^{4/3})}{3}\right]^{1/4} \mu_2. \tag{2.17}$$

Hence, the total baryon number in this case can be written as

$$\rho_3 = \frac{\mu_3^3}{\pi^2} = \left[\frac{(1+2^{4/3})}{3}\right]^{3/4} \rho_2. \tag{2.18}$$

The energy per baryon is then given by

$$\left(\frac{E}{A}\right)_3 \equiv \frac{\epsilon_3}{\rho_3} = \frac{4B}{1.127\rho_2} = 829MeV \times B_{145}^{1/4}, \tag{2.19}$$

since $\epsilon_3 = 3P_3 + B = 4B = \epsilon_2$. We thus see that the energy per baryon of a massless non-interacting 3-flavor quark gas is of order 100 MeV per baryon, *lower* than in 2-flavor quark matter. The difference arises from,

$$\frac{\rho_2}{\rho_3} = \left[\frac{3}{(1+2^{4/3})}\right]^{3/4} \approx 0.89, \tag{2.20}$$

which reflects that the baryon number can be packed more densely into 3-flavor quark matter ($\rho_3 > \rho_2$) due to the extra Fermi well accessible to the strange quarks.

To compare, the energy per baryon in a free gas of neutrons is the neutron mass, $E/A = m_n = 939.6$ MeV. For a $^{56}$Fe nucleus, one has $E/A = (56m_N - 56.6\ MeV)/56 \approx 930$ MeV, where $m_N$ denotes the nucleon mass. Thus, stability of $u$,$d$,$s$-quark matter is *absolutely* stable relative to $^{56}$Fe that corresponds to $(E/A)_3 < 930$ MeV (Weber, 2017). If the strange matter hypothesis is true, there could exist large pieces of stable SQM called strange quark stars (with the baryon number $A \sim 10^{57}$) (Alcock et al., 1986; Baym and Chin, 1976) and, small SQM nuggets (with $A \leq 10^7$) often referred as *strangelets* (Farhi and Jaffe, 1984; Berger and Jaffe, 1987, 1991; Madsen, 1993) or *slets* (Peng et al., 2006). Thus, the basis throughout our work is the strange quark matter hypothesis. Next, we will study strangelets and their mass formula.

## 2.3 Strangelets: Mass Formula

As mentioned in the previous section, we assume the true ground state of matter consists of a combination of up, down, and strange quarks known as "strange quark matter" (SQM). Small nuggets of such matter are called "strangelets". Strangelets (dimensions of a few Fermis) have been investigated by Farhi and Jaffe (1984); Berger and Jaffe (1991); Madsen (1993). They have calculated the mass formula for strangelets and, in particular, they have derived the charge $Z$ and radii $R$ of strangelets which are given in terms of the baryon number $A$ when the $SQM$ is in $\beta$ equilibrium. They did, however, make the assumption that the strangelets are uniformly charged, i.e., the chemical potential is not spatially varying within the quark matter strangelet. Nevertheless, Heiselberg (1993) showed up that this is inconsistent, since the electrostatic potential will then be increasing towards the center and the quarks will migrate due to the electric field. He took into account the screening effect[5] in strangelets and found a more refined mass formula for large droplets with baryon number $A \gtrsim 10^5$.

In general, a strangelet with radius $R$ will have charge distributions that vary on the scale of the Debye screening length $\lambda_D$[6]. When $\mu_i \sim \mu$ the screening length is $\lambda_D \simeq 7/\mu$, almost independent of the strange quark mass. Taking a typical value for the quark chemical ($\mu \simeq m_N/3 \simeq 300$ MeV, $m_N$ is the nucleon mass), one find $\lambda_D \simeq 5$ fm (Heiselberg, 1993). Thus, we follow Heiselberg (1993) where the screening will be taken into account and the spatially varying chemical and electrostatic potentials will be found in Heiselberg (1993). Consequently, the correct mass formula, radii, and charge are calculated. Quark screening will reduce the strangelet charge and hence this scenario is not energetically favored for strangelets of sizes larger than the quark screening length as shown in Heiselberg (1993). Heiselberg (1993) found that if the characteristic spacial scales of the structures are less than about 10 fm for the nuclear phase, and less than $\sim 5$ fm for the quark phase, screening effects will be unimportant, and the electron density will be essentially uniform. In the opposite case, when screening

[5]Screening effect is also known as the shielding effect. The phenomenon which occurs when the nucleus reduces its force of attraction on the valence electrons due to the presence of electrons in the inner-shell. This is known as a screening effect. Outer electrons experience attraction from the nucleus and repulsion from the inner electrons.

[6]The Debye length (also called Debye radius), is a measure of a charge carrier's net electrostatic effect and how far its electrostatic effect persists. With each Debye length, the charges are increasingly electrically screened, and the electric potential decreases (Shohet, 2003).

lengths are short compared with spatial scales, the total charge densities in bulk[7] nuclear matter and quark matter will both vanish. For the case when screening lengths are much larger than the spatial scale structures. This later condition implies that the electron density is uniform everywhere, and all other particle densities are uniform within a given phase (Heiselberg, 1993).

We implement the Heiselberg's improved mass formula for strangelets as suggested in Heiselberg (1993). The *MIT* bag model is a widely used approximation to describe the bulk properties of quark matter. For simplicity $\alpha_c = 0$[8], this implies that: the chemical potentials are just the Fermi energies, the effects of gluons on the dispersion relation for the quarks can be neglected, as well as the Landau-Fermi-liquid interactions among quasi-particles. Only strangelets of a size less than typical atomic distances will be studied in order to avoid the presence of electrons in the bulk quark matter; i.e., we can assume that $\mu_e \simeq 0$. This restricts the strangelet radial size to $R \gg a_B/Z$ ($Z$ is the strangelet charge) and, an upper limit on the baryon mass number $A = (4\pi/3)R^3 n_B$, where $n_B$ is the baryon density. The charge $Z$ is increasing with strangelet size and depends strongly on the strange quark mass $m_s$. In addiction, the charge as a function of mass number will be calculated for different values for $m_s$. For small $m_s$ the charge density and therefore $Z$, is very small because the charge of the $u$ quark $(+2e/3)$ is almost balanced by the charges of $d$ and $s$ quarks $(-e/3)$. Therefore, $A$ can be large without electrons being present in the strangelets. For large $m_s$, the condition $A \gg 10^5$ must be satisfied in order to avoid electrons in the bulk quark matter.

Heiselberg found that the total charge $Z$ of the strangelet is Heiselberg (1993)

$$Z = \frac{1}{\alpha} R\Delta\mu \left(1 - \frac{tanh(Rq_D)}{Rq_D}\right), \tag{2.21}$$

where $R = aA^{1/3}/\mu_0$ with $a \simeq 1.4$ and $\mu_0 \simeq 300$ MeV; $\alpha \approx 1/137$; $q_D = \lambda_D^{-1}$ where $\lambda_D \simeq 7/\mu$ is the Debye screening length (when $\mu_i \sim \mu$, where $i = u, d, s$). Recall that we can safely adopt $\mu \simeq \mu_0$. In addition, $\Delta\mu$ is defined by

$$\Delta\mu = \begin{cases} m_s^2/\mu, & m_s \ll \mu, \\ \mu/5, & m_s \geq \mu. \end{cases}$$

[7] Consider a body which has a finite volume and surface area. Bulk means, the region of a body in which the physical properties of the body are not influenced by its surface area.

[8] $\alpha_c$ is the strong interaction coupling constant.

With these equations above, we can find $Z(A)$. Heiselberg also found the total energy per quark given by

$$\frac{E}{N} \simeq \mu_0 + \frac{E_S + E_C}{N_0} \tag{2.22}$$

where $N$ is the number of quarks in the strangelet; $N_0 = n(\mu_0)V$, with $V = (4\pi/3)R^3$; $E_S = 4\pi\sigma R^2$ is the surface energy ($\sigma$ is the surface tension constant here); and $E_C$ is the Coulomb energy of the strangelet given by

$$E_C = \frac{\Delta\mu^2 R}{2\alpha}\Big[1 - \frac{3}{2}\frac{tanh(Rq_D)}{Rq_D} + \frac{1}{2}cosh^{-2}(Rq_D)\Big], \tag{2.23}$$

Thus, the final mass formula described by Heiselberg can be written as (Heiselberg, 1993):

$$\frac{E}{N} = \mu_0 + \frac{E_C + 4\pi\sigma R^2}{4\pi R^3(n/3)}, \tag{2.24}$$

where $\mu_0 = \mu_d = \mu_s = \mu_u$ due to $\beta$ equilibrium, $R$ is the strangelet radius, $\sigma$ is the surface tension, $n$ is the quark density, and $E_c$ is the Coulomb energy. Note that

$$\frac{E}{N} = \frac{E}{3A}, \tag{2.25}$$

and the quark number density is[9]

$$n(\mu_0) = \frac{\mu_0^3}{\pi^2}\begin{cases} 3\left(1 - \frac{m_s^2}{2\mu_0^2}\right), & m_s \ll \mu_0, \\ 2, & m_s \geq \mu_0. \end{cases}$$

As we will see in chapter 3, we are interested in crystalline strange matter, thus we need to restrict our study to the low-surface-tension regime. As discussed in Alford et al. (2012), the critical value for the surface tension that allows the formation of a strangelet crystal structure is $\sim 1 - 10$ MeV $fm^{-2}$, which is appropriate for the scenario we are interested in. Thus, we use $\sigma = 0.6$ MeV.$fm^{-2}$. We can compute the properties of some strangelets in the Table 2.3. Note that we have also calculated strangelet properties for $\sigma = 0.2 - 1.0$ MeV $fm^{-2}$, which did not significantly change the strangelet energy. By providing different values for $A$ and using Eq. (2.21) to calculate the charges of different strangelets, whose properties we present in Table 2.3. The strangelets that we use

[9]Here we will use $m_s = 150$ MeV.

in our work are appropriate to describe the low-pressure planetary-like objects that we are interested in.

Table 2.1: Properties of some strangelets from equation (2.24) for different constant surface tension values $\sigma$ (in $MeVfm^{-2}$).

| Label | A | Z | E(A,Z) ($10^6$ MeV) | | |
|---|---|---|---|---|---|
| | | | $\sigma = 0.2$ | $\sigma = 0.6$ | $\sigma = 1.0$ |
| $Stra_1$ | $5 \times 10^3$ | 581 | 4.5176 | 4.5189 | 4.5201 |
| $Stra_2$ | $1 \times 10^4$ | 793 | 9.0258 | 9.0277 | 9.0297 |
| $Stra_3$ | $5 \times 10^4$ | 1527 | 45.055 | 45.060 | 45.066 |
| $Stra_4$ | $1 \times 10^5$ | 1986 | 90.073 | 90.082 | 90.091 |

As expected, strangelets with higher $A$ have larger masses, furthermore, the $Z/A$ ratio is small relative to ordinary nuclei, as strangelets are less charged (due to the presence of the negatively charged strange quark). In this context, following Heiselberg (1993), in chapter 3 we explore the possibility of planet-like objects made up of nuggets of SQM arranged in a crystal lattice, considering Alford et al. (2012). Their orbital properties are investigated and their possible detection. Next, we consider the possibility that quark stars would have a strangelets crust.

## 2.4 Possibles Strangelet Crusts on Quarks Stars' Surfaces

The possibility that strange star surfaces have crusts was pointed out by Alcock et al. (1986); Haensel et al. (1986a). Additionally, it has been pointed out that under certain conditions, the surface of a strange star may be crusted with a crystal of charged strangelets in a neutralizing background of electrons (Jaikumar et al., 2006; Alford et al., 2006). They investigated the possibility for realizing a heterogeneous crust (nuggets of strange quark matter + electrons). This phase resembles the mixed phase of nuclei and electrons in the crusts of normal neutron stars, where electrons contribute to the pressure while quarks contribute to the

energy density (Jaikumar et al., 2006). Later, a more careful calculation of the properties of a strangelet crystal crust was made by Alford and Eby (2008). In the face of this, here, we consider the possibility that quark stars may be crusted with strangelets as proposed by Jaikumar et al. (2006); Alford et al. (2006).

The first proposal for a crust on the strange stars was made in Alcock et al. (1986) where quark stars could have a tiny nuclear crust suspended a few hundred Fermis above the quark star, supported by large electric fields near the surface. Besides, in Haensel et al. (1986a) mentioned the possibility of crust nuggets, not even a qualitative study of its consequences exists. It was Jaikumar et al. (2006) who developed the first quantitative study of a crust with strangelets. They analyzed the surface region of strange stars and found that heterogeneous (solid) crust made of strange nuggets and electrons may be possible. To prove that, they proposed that a heterogeneous mixed phase with nuggets and electrons may be favored if the surface and Coulomb energy costs are small. Deeper in the crust, that mixed phase[10] is characterized by voids filled by an electron gas embedded in quark matter. This mixed phase resembles the mixed phase of nuclei and electrons in the crust of normal neutron stars where, electrons contribute to the pressure while quarks contribute to the energy density.

Assuming that the crust is in a non-superconducting, globally neutral mixed phase of strangelets and electrons, we follow the configuration described in Jaikumar et al. (2006) which has stable strangelets coexisting with electrons.

Hence, the pressure is only due to electrons by

$$P_{crust} = \frac{\tilde{\mu}_e^4}{12\pi^2}, \quad \tilde{\mu_e} = \frac{n_Q}{\chi_Q}\left(1 - \sqrt{1-\xi}\right), \quad \xi = \frac{2P_0\chi_Q}{n_Q^2}, \tag{2.26}$$

where

$$n_Q = \frac{m_s^2\mu_q}{2\pi^2}, \tag{2.27}$$

and

$$\chi_Q = \frac{2\mu_q^2}{\pi^2}, \tag{2.28}$$

represent the quark charge and quark susceptibility, respectively, and $P_0$ is the pressure of electron-free quark phase. $\mu_q$ is the quark chemical potential.

[10] At low temperature, the mixed phase is a solid

While the energy density is due to the nuggets, and is given by,

$$\epsilon = x\epsilon_0, \tag{2.29}$$

where $x$ is the volume fraction of the quark phase given by

$$x = \frac{\tilde{\mu}_e^3}{3\pi^2 n_Q}\left(1 - \frac{\chi_Q \tilde{\mu}_e}{n_Q}\right)^{-1}, \tag{2.30}$$

and $\epsilon_0$ denotes the energy density inside nuggets (see Jaikumar et al. (2006) for more details of the terms). In this first study, we have chosen this model of strangelets crust due to its simplicity. To ascertain if strange nuggets are indeed stable with respect to fusion at low pressure requires a proper account of Debye screening and curvature energy. If theses are small enough, then almost all strange stars should have a crust and strangelets at zero pressure should have a finite stable size (Jaikumar et al., 2006; Alford et al., 2006; Alford and Eby, 2008). We explore in chapter 4 the consequences of the presence of a crust of strangelets on the cooling calculations and thermal relaxation of those quark stars.

## 2.5 The Equation of State for Strange Quark Matter

Finally, here we study the equation of state (EOS) for strange quark matter, that is, the relationship between pressure and energy density. The EOS is fundamental to determining the macroscopic properties of stars, such as radii and masses. The most prominent models used to describe strange quark matter is the model known as *MIT* bag model (Farhi and Jaffe, 1984; Chodos et al., 1974b,a; Weber et al., 2009). In this thesis, we will describe quark matter using the *MIT* bag model for massive strange quarks and with first order corrections in $\alpha_c$ (the strong interaction coupling constant).

We describe strange quark matter as a degenerate gas of fermions composed of up, down and strange quarks, along with electrons. The chemical equilibrium is maintained by weak-interaction processes:

$$d \leftrightarrow u + e + \bar{\nu_e},$$

$$s \leftrightarrow u + e + \bar{\nu_e},$$

$$s + u \leftrightarrow u + d.$$

From these relations, it follows that at equilibrium the chemical potential obey:

$$\mu_d = \mu_s \equiv \mu, \tag{2.31}$$

$$\mu_u + \mu_e \equiv \mu, \tag{2.32}$$

we set $\mu_i$, for $i = u, d, s$ and $e$ as the chemical potential for the up, down and strange quarks and, the electron, respectively. Equations (2.31)- (2.32) imply that there are only two independent chemical potentials ($\mu_s$ and, $\mu_e$ for instance). On the other hand, the neutrinos play no role for the composition of equation of state (they will be very important later) and therefore are ignored for now.

The Landau potential is written as

$$\Omega = U - TS - \mu N, \tag{2.33}$$

where $U$ is the internal energy density, $T$ is the temperature, $S$ is the entropy density, $\mu$ is the chemical potential, and $N$ is the particle density. Here, we consider first order correction in $\alpha_c$, which is the coupling constant for the quark-quark interaction. We also consider a finite mass for the strange quark ($m_s$). The quarks and electron Landau potential with first order corrections in $\alpha_c$ and for massive $s$ quarks are given by (Farhi and Jaffe, 1984)

$$\Omega_u = -\frac{\mu_u^4}{4\pi^2}\left(1 - \frac{2\alpha_c}{\pi}\right), \tag{2.34}$$

$$\Omega_d = -\frac{\mu_d^4}{4\pi^2}\left(1 - \frac{2\alpha_c}{\pi}\right), \tag{2.35}$$

$$\Omega_e = -\frac{\mu_e^4}{12\pi^2}, \tag{2.36}$$

$$\Omega_s = -\frac{1}{4\pi^2}\left\{\mu_s\sqrt{\mu_s^2-m_s^2}\left(\mu_s^2-\frac{5}{2}m_s^2\right)+\frac{3}{2}m_s^4\ln\left(\frac{\mu_s+\sqrt{\mu_2^2-m_2^2}}{m_2}\right)\right.$$
$$-\frac{2\alpha_c}{\pi}\left[3\left(\mu_s\sqrt{\mu_s^2-m_s^2}-m_s^2\ln\left(\frac{\mu_s+\sqrt{\mu_s^2-m_s^2}}{m_s}\right)\right)^2-2(\mu_s^2-m_s^2)^2\right.$$
$$\left.\left.+3m_s^4\ln^2\frac{m_s}{\mu_s}+6\ln\frac{\Sigma}{\mu_s}\left(\mu_s m_s^2\sqrt{\mu_s^2-m_s^2}-m_s^4\ln\left(\frac{\mu_s+\sqrt{\mu_s^2-m_s^2}}{m_s}\right)\right)\right]\right\}. \tag{2.37}$$

In equation (2.37) $m_s$ is the strange quark mass and $\Sigma$ is a renormalization constant, whose value should be of the typical order of the chemical potentials. In this study, we set $\Sigma = 300$ MeV.

The number density of each species is given by

$$\rho_i = -\frac{\partial\Omega_i}{\partial\mu_i}, \tag{2.38}$$

with $i = u, d, s, e$. As is usually assumed to be the case for a bulk system, charge neutrality must be imposed. The charge neutrality equation is given by

$$\sum_{i=u,d,s,e} q_i\rho_i = \frac{2}{3}n_u - \frac{1}{3}n_d - \frac{1}{3}n_s - n_e = 0, \tag{2.39}$$

combining equation (2.39) with equations (2.31) and (2.32) leaves only one independent chemical potential, which we chose to be $\mu$. In the *MIT* bag model, the particles are assumed to exist inside a bag. The energy density of the fermions needs to be complemented by the energy density associated with the bag, in this way the expression for the energy density is given by

$$\epsilon = \sum_{i=u,d,s,e}(\Omega_i + \mu_i\rho_i) + B, \tag{2.40}$$

where $B$ is the bag constant. In the same way, the pressure of fermions is counterbalanced by the pressure of the bag, and thus the expression for the pressure is

$$p = -B - \sum_{i=u,d,s,e}\Omega_i \tag{2.41}$$

In the limit, when $\alpha_c \to 0$ and $m_s \to 0$, we obtain the simple analytical equation

of state given by

$$p = \frac{\epsilon - 4B}{3} \tag{2.42}$$

It is important to mention that more sophisticated quark models have been proposed in Nambu and Jona-Lasinio (1961a,b); Fukushima (2003, 2004); Ratti et al. (2006) (and reference therein) as well there has been great improvement in the bag model, accomplished by modern perturbation calculations, see for instance Fraga et al. (2014). We note, however, that such improved and more sophisticated models lead to qualitatively similar compositions, thus it is unlikely that they would strongly modify the thermal evolution, which is the focus of chapter 4.

## 2.6 Summary

In this chapter, we have presented our basis of this thesis, that is, the strange quark matter (SQM) hypothesis, the strangelets mass formula and the possibility of strangelets crust on the surface of quark stars, and the equation of state for strange quark matter. According to strange quark matter (SQM) hypothesis, strange matter which contains, roughly equal numbers of up, down and strange quarks may be the ground state of the strong interaction (Bodmer, 1971; Witten, 1984; Terazawa, 1979), that is, strange quark matter may have an energy per baryon that is less than that of nuclear matter. If true, strange matter could exist from small lumps of strange matter called strangelets to large compact stars made entirely of strange matter. In the next chapter, we assume the SQM hypothesis and explore the possible existence of planet-like objects made of a crystal–strangelets structure following Alford et al. (2012) and Heiselberg (1993), as well as to discuss their orbital properties, we call them strangelet crystal planets (Zapata and Negreiros, 2020). Next, in chapter 4, we focus our attention by studying quark stars surrounded by a crust comprised of strangelets embedded in a uniform electron background following Alcock et al. (1986), Jaikumar et al. (2006), and the strange quark matter equation of state (section 2.5). We will also include their thermal properties and compare them with quark stars crusted by ordinary nuclear matter (Zapata, J. et al., 2022). We can argue a possible sequence of compact objects that consist a core of strange matter enveloped within strangelet crystal planets matter. Specially, we focus on planetary-like objects and quark stars with strangelets crust.

Chapter 3

# Strangelets Crystal Planets

## 3.1 Introduction

We begin this chapter considering the possibility that strange quark matter (SQM) may manifest in the form of strangelet crystal planets (Zapata and Negreiros, 2020). These planet-like objects are made up of nuggets of SQM, organized in a crystalline structure. We assume the so-called strange matter (SQM) hypothesis proposed by Bodmer (1971); Witten (1984); Terazawa (1979). In this context, we analyze planets made up entirely of strangelets arranged in a crystal lattice (Heiselberg, 1993; Alford et al., 2012). Furthermore, we proposed that a solar system with a host compact star may be orbited by strangelet crystal planets. Under this assumption, we calculate the relevant quantities that could potentially be observable, such as the planetary tidal disruption radius[1], and the gravitational-wave signals that may arise from potential star-planet merger events (Huang and Yu, 2017; Geng et al., 2015). Our results, under hypothesis, shown that strangelet crystal planets[2] could potentially be used as an indicator for the existence of SQM (Zapata and Negreiros, 2020).

Under the SQM hypothesis, compact stars can be considered strange quark stars, self-bound objects composed of SQM, as opposed to traditional, gravitationally bound neutron stars (Witten, 1984; Alcock et al., 1986; Haensel et al., 1986b). Furthermore, in Witten (1984); Alcock et al. (1986); Glendenning et al. (1995); Haensel et al. (1986b); Kettner et al. (1995), the authors further developed the concept of strange quark stars, that is, objects consisting of a SQM

[1] Tidal disruption radius $r_{td}$ is the critical distance at which the tidal force is exactly balanced by the self-gravity of the planet. If the distance is smaller than $r_{td}$, the tidal force will dominate and the planet will be completely broken up.

[2] The work of this chapter was published in Zapata and Negreiros (2020).

core surrounded by nuclear crust. They found a complete sequence of strange stars that range from very compact members, with properties similar to those of neutron stars, to white dwarfs-like objects (strange dwarfs), to planetary-like strange matter objects. It was pointed out that the minimum-mass configuration in such a sequence is $\sim 0.017M_\odot$, and that such values depend on the chosen value of inner crust density (Glendenning et al., 1995; Kettner et al., 1995). If abundant enough in our Galaxy, such low-mass strange stars, whose masses and radii resemble those of ordinary planets, could be seen by gravitational microlensing searches (Weber et al., 1996). Furthermore, Alford et al. (2012) performed a study on *strangelet dwarfs*, which consist of a crystalline structure of strangelets in a sea of electrons. In their work, they showed that if the surface tension of the interface between strange matter and the vacuum is less than a critical value, there is, at least, one stable branch in the mass-radius relation for strange stars.

In this chapter, we follow the work of Alford et al. (2012), except we focus on planetary objects characterized by low pressures. In addition, recently there have been great advances in the detection of exoplanets with a wealth of data available (Perryman, 2000; Schneider et al., 2011; Armstrong et al., 2016; Borucki, 2016). Recently, Huang and Yu (2017) and Geng et al. (2015) proposed the use of such data to search for strange quark matter (SQM) planets (in the context defined by Kettner et al. (1995); Glendenning et al. (1995)) by analyzing two possible observational signatures: the tidal disruption radius and the gravitational–waves (GWs) emission from a binary system composed of a host compact star and a strange planet. They identified candidates of SQM planets using the following specifications: very small orbital period ($< 6100$ s), and orbital radius smaller than $5.6 \times 10^{10}$ cm, and possible strong GW emission by strange planets with masses $> 10^{-5}M_\odot$. The idea is that if any of these planets are, in fact, strange planets, then due to their strange matter properties (increased compactness, for instance) their observational signatures should be different. In this first chapter, we also follow in the footsteps of Huang and Yu (2017); Geng et al. (2015) by searching for signatures of SQM in the observed data of exoplanets. We consider, however, a somewhat more sophisticated model for strange quark planets, one that resembles the actual structure of a planet. We recall that in the original proposal, strange planets were in fact very low-mass strange stars (the order of a few Jupiter masses), with a small seed of strange matter in its core and a relatively large nuclear crust extending all the way to the surface. In our model, as will become clear, we consider the possibility of strangelets forming a

crystalline structure such that, as in a white dwarf, the objects are supported against gravitational collapse by electron degeneracy pressure. Differing from a white dwarf (or the crust of neutron stars), in our proposed model instead of ions we have strangelets. Such objects could be formed by the same process that hypothetically generated the compact star host (in a supernova, or stellar merger event, for instance), with the high-density matter giving birth to the high-density strange quark star (composed of homogeneous strange matter) and lower-density lumps, giving rise to crystalline strange planets.

This chapter is divided as follows: first, we will describe the microscopic model for strangelet crystal planets made up strangelets following the section 2.3 and then, we calculate the equation of state (EOS) of strangelet crystal matter. Later, the EOS allows us to compute the structure of the strangelet crystal planets by imposing the appropriate hydrostatic equilibrium conditions in such manner, we get the sequences of planet-like objects that we call strangelet crystal planets (SCPs). Next, we investigate the orbital properties of the SCPs and discuss their possible observational implications. Finally, we argue their possible applications to sub-stellar objects.

## 3.2 Microscopic Model: Equation of State

Here, we follow Glendenning (2012) to do a simple calculation of the equation of state of planet-like objects consisting of a single nuclear species. Only, instead of a single nuclear species, we consider strangelets as described in the section 2.3. Except at the very lowest densities, we can consider the lowest approximation, that is, a fully ionized strangelets immersed in a background of uniform density electrons. The positively strangelet charged will arrange themselves into a lattice with the strangelet at the lattice sites to minimize the Coulomb energy (Wigner–Seitz approximation, see the Fig. 3.1); that is, by considering a sphere surrounding each nucleus and touching the neighboring spheres (there is no interaction between spheres). Each sphere containing a strangelet and its electrons will be neutral.

For one of them, most of the mass is contributed by strangelets, whereas most of the pressure by the electrons (Glendenning, 2012). The energy in each sphere consists of the strangelet mass, the electron mass and kinetic energy, the energy of Coulomb repulsion among the electrons, and the attractive Coulomb

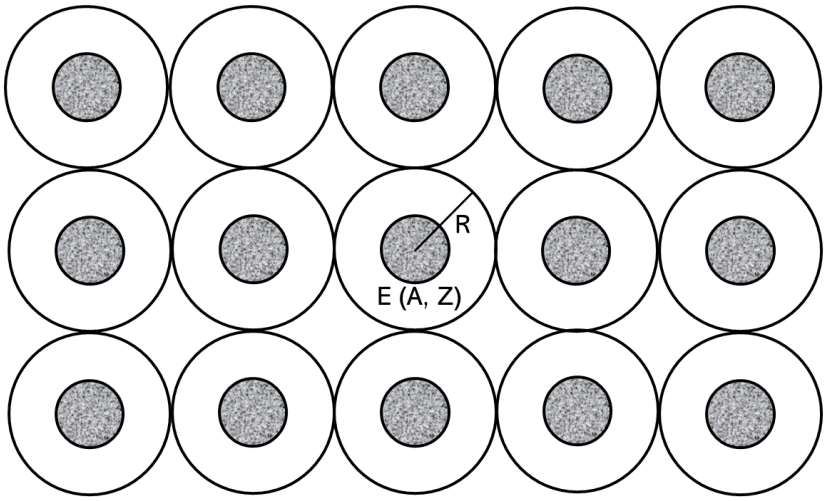


Figure 3.1: Illustration of Wigner–Seitz approximation. In this graphic representation, we have a crystal structure of a strangelet $E(A, Z)$. At the center of each sphere is the strangelets surrounded by an electron cloud. $R$ is the cell's radius.

energy between the electron sea and the strangelets.

The Coulomb energy needed to assemble the electrons into the cell of radius $R$ is known. We need to integrate the interaction between the charge within radius $r$ and the charge in a shell at $r$ of thickness $dr$ (Glendenning, 2012),

$$E_{self} = e^2 \int_0^R \frac{1}{r} \left( \frac{4\pi r^3}{3} \rho_e \right) \left( 4\pi r^2 dr \rho_e \right), \tag{3.1}$$

where the electron number density is given by $\rho_e = Z/V$, and

$$V = \frac{4\pi R^3}{3}, \tag{3.2}$$

with $Z$ the atomic number of the strangelets and therefore the electron number per cell. The electron gas will have an attractive interaction with the strangelet at the center of the cell,

$$E_{int} = -\int \frac{1}{r}(Ze)(4\pi r^2 dre\rho_e) = -\frac{3(Ze)^2}{2R} \tag{3.3}$$

Thus, the total Coulomb energy of the cell is

$$E_{lat} = E_{self} + E_{int} = -\frac{9(Ze)^2}{10R}. \tag{3.4}$$

Using $Z = V\rho_e$ and $V = 4\pi R^3/3$, we have the lattice contribution to the pressure,

$$P_{lat} = -\frac{\partial E_{lat}}{\partial V} = -\frac{3}{10}\left(\frac{4\pi}{3}\right)^{1/3} Z^{2/3} e^2 \rho_e^{4/3}. \tag{3.5}$$

We may choose a baryon density $\rho$ in which case the cell radius $R$ is given by

$$A = \frac{4\pi R^3 \rho}{3}, \tag{3.6}$$

where $A$ is the baryon mass number of the strangelets and $Z$ is the strangelet charge. For a chosen density $\rho$, the electron density is

$$\rho_e = \left(\frac{Z}{A}\right)\rho, \tag{3.7}$$

and, we treat the free electrons as a degenerate Fermi gas with maximum wave number

$$k_e = (3\pi^2 \rho_e)^{1/3}. \tag{3.8}$$

Denoting the corresponding energy density and pressure by $\epsilon_e(k_e)$ and $P_e(k_e)$, respectively, given in Appendix B. The energy density is

$$\epsilon = \frac{E_{total}}{V}, \tag{3.9}$$

with $V = A/\rho$. So the energy density and pressure are

$$\epsilon(\rho) = \frac{\rho}{A}\left(E(A,Z) - Zm_e - \frac{9(Ze)^2}{10R}\right) + \epsilon_e(k_e), \tag{3.10}$$

$$P(\rho) = P_e(k_e) - \frac{3}{10}\left(\frac{4\pi}{3}\right)^{1/3} Z^{2/3} e^2 \rho_e^{4/3}, \tag{3.11}$$

where $E(A,Z)$ is the strangelet mass, $e$ is the charge of electrons, and $\epsilon_e(k_e)$ and $P_e(k_e)$ are the energy density and pressure of electrons, respectively (according to equations (B.1) from Appendix B). This equation of state cannot be valid above the density at which high-energy electrons are capture (neutronization processes by inverse beta decay). At higher densities, the lattice contribution to pressure

become important. On the other hand, to estimate the lower density range at which the approximation of fully ionized nuclei is valid, we use the limit non–relativistic electrons from Glendenning (2012), this predicts that $P = 0$ when the baryon densities should satisfy

$$\rho > \frac{3Z^4}{2\pi}\frac{1}{r_{Bohr}^3}$$

or energy densities

$$\epsilon > 5.4Z^4 \ (g.cm^{-3}) \tag{3.12}$$

where $r_{Bohr} = \text{~}^2/m_e e^2$ is the Bohr radius of the inner orbit of the atomic species. Note that for the low-pressure regime we consider here, the energy density is mostly dominated by the $E(A, Z)$ contribution. The negative term on equation (3.11) is the lattice contribution to the total pressure. Furthermore, the third term on equation (3.10) represents electrostatic correction to the total energy density[3]. Recalling that strangelets were discussed in the section 2.3 and their properties are in table 2.3. Thus, we adopt here the Wigner–Seitz approximation, much like in Alford et al. (2012) and then, we consider a crystal structure of periodic spheres in which each cell of radii $R$ consists of a strangelet residing at its center, surrounded by an electronic cloud (see Fig. 3.1). Each cell contains the amount of electrons needed to make it electrically neutral (Glendenning, 2012; Shapiro and Teukolsky, 2008). As we have mentioned before, we are interested in planetary objects characterized by low pressure/density, thus the constant electron density approximation is appropriate (Alford et al., 2012), and we ignore the effect of pressure when calculating the strangelet properties, in particular $Z(A)$.

The EOS of such matter is represented in Figure 3.2 from Eqs. (3.10)-(3.11), where we have used the $E(A, Z)$ for strangelets masses from table 2.3. In that figure, we show the pressure as a function of energy density for the EOS associated with each of the studied strangelets.

As we can note in that figure, the crystalline matter proposed for planet-like objects have relatively low densities and pressure (in particular when compared to other works dealing with SQM (Alford et al., 2012)). We might intuitively think that larger strangelet masses correspond to massive objects, but we found the opposite. As we can observe in that figure, less massive strangelets (as the $\text{stra}_1$

[3]Note that as in Heiselberg (1993), we are using $e^2 = \alpha$, the fine structure constant.

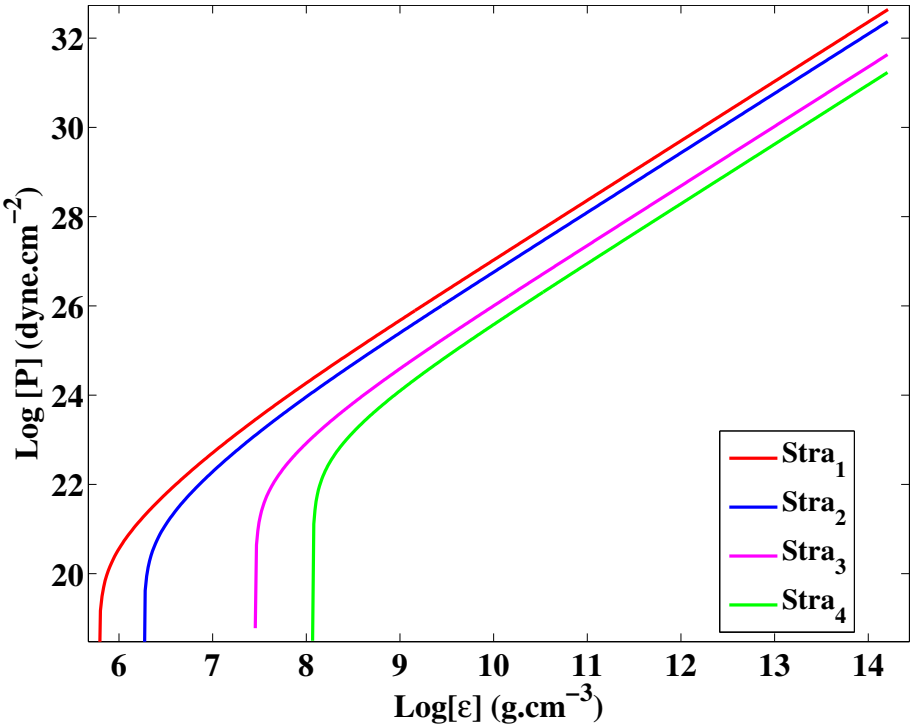


Figure 3.2: Equations of state for strangelet crystal planets made of different strangelet labeled as "Stra" from Table 2.3 and Eqs. (3.10)-(3.11).

label) are associated with "stiffer" equation of state, i.e., higher pressures at the same energy density. This can be understood from an analysis of the $Z/A$ ratio that appears in equation (3.7) for electron density. Fixing the baryon density, $\rho$, as $A$ increases, the number of electrons that contribute to the pressure decreases, so we have a reduction in pressure. As a consequence, massive strangelets (larger $A$) correspond to lower-mass planetary objects. Whereas, strangelets with less $A$ correspond to objects of greater mass. This will be evident in the next section.

## 3.3 Strangelet Crystal Planets

### 3.3.1 Tolman–Oppenheimer–Volkoff Equations

With the complete description of the microscopic physics (last section), we now proceed to determine the macroscopic properties of self-gravitating objects. For this study we use the structure equations of a non-rotating, static spherically symmetric objects[4].

The metric of such an object has the form (Weber, 2017)

$$ds^2 = -e^{2\Phi(r)}dt^2 + e^{2\Lambda(r)}dr^2 + r^2 d\Omega^2 \tag{3.13}$$

where $\Phi(r)$ and $\Lambda(r)$ are the radially metric functions and, $d\Omega$ is given by

$$d\Omega^2 = d\theta^2 + \sin^2\theta d\phi^2. \tag{3.14}$$

With the aid of Einstein's equation and assuming that the matter is a perfect fluid[5], one gets the Tolman-Oppenheimer-Volkoff (TOV) equation (Oppenheimer and Volkoff, 1939; Tolman, 1939), which represents the hydrostatic equilibrium equation of a spherical body given by

$$\frac{dP}{dr} = -\frac{[\epsilon(r) + p(r)][m(r) + 4\pi r^3 p(r)]}{r(r - 2m(r))}, \tag{3.15}$$

with the central pressure $P(r = 0) = P(\epsilon_c)$ and $\epsilon_c$ as the star's central mass energy density. The quantities $\Phi(r)$ and $\Lambda(r)$ are given by

$$e^{-2\Lambda(r)} = 1 - \frac{2m(r)}{r} \tag{3.16}$$

and

$$\frac{d\Phi(r)}{dr} = \frac{4\pi r^3 P + m(r)}{r^2(1 - 2m(r)/r)}. \tag{3.17}$$

Equation (3.15) is fundamental to the description of the structure of a hydrostatically stable stellar configuration treated in the framework of Einstein's theory, which needs to be solved in conjunction with the mass continuity equa-

[4] see Appendix C

[5] A perfect fluid in relativity is defined as one that has neither viscosities nor heat conduction in the frame of reference that moves along with the fluid.

tion,

$$\frac{dm(r)}{dr} = 4\pi r^2 \epsilon(r) \tag{3.18}$$

for a particular equation of state, $P = P(\epsilon)$. In the classical limit one has $P << \epsilon$, $P << m$, and $2m/r << 1$ in (3.15), which leads to a pressure gradient given by

$$\frac{dP}{dr} = -\frac{\epsilon(r)m(r)}{r^2} \tag{3.19}$$

This relation revels that Einstein's theory increases (the magnitude of) the pressure gradient over what one obtains from the Newtonian treatment, which is quite crucial for stellar bodies.

Let us see how this comes out when integrating (3.15). First, one has to specify a model for the equation of state in the form $P(\epsilon)$ and a value of central density $\epsilon_c$. This determines $P_c$ while $dP/dr$ and $m$ vanish at $r = 0$. Equation (3.18) then determines $m$ for an infinitesimal increase in $r$. In this way, the computation of $P$, $\epsilon$, and $m$ for successively increasing values of $r$ goes on until we arrive at $P = 0$, which is identified as the radius, $R$, of the star, and the value $m$ there is the star's total mass–energy, $M$. The metric function $\Phi$ can be obtained by simultaneously integrating (3.17) too. The iteration of equation (3.15) is repeated for different values of $\epsilon_c$, leading each time to a particular relativistic stellar model, whose structure functions $m$, $\epsilon$, $P$, $\rho$ (and $\Phi$, if desired) satisfy the equations of stellar structure. Notice that for any fixed choice of equation of state, $P(\epsilon)$ or $P = P(\rho)$, $\epsilon = \epsilon(\rho)$, the stellar models form a *one-parameter* sequence (parameter $\epsilon_c$). Once the central density has been specified, the model is determined uniquely. In the next section, we will solve the TOV's equation to find the sequence of planets-like objects.

### 3.3.2 Sequence of Strangelet Crystal Planets

We now employ the EOS developed in Section 3.2 for a strangelet crystal configuration to obtain the macroscopic properties of such objects. Since we are considering a solid, fully crystallized object, we found it appropriate to name them strangelet crystal planets, to differentiate them from previous models of strange planets (in which SQM is not crystallized, but present in bulk in a small region of the object's core (Alcock et al., 1986; Glendenning et al., 1995; Kettner et al., 1995; Alcock and Olinto, 1988)).

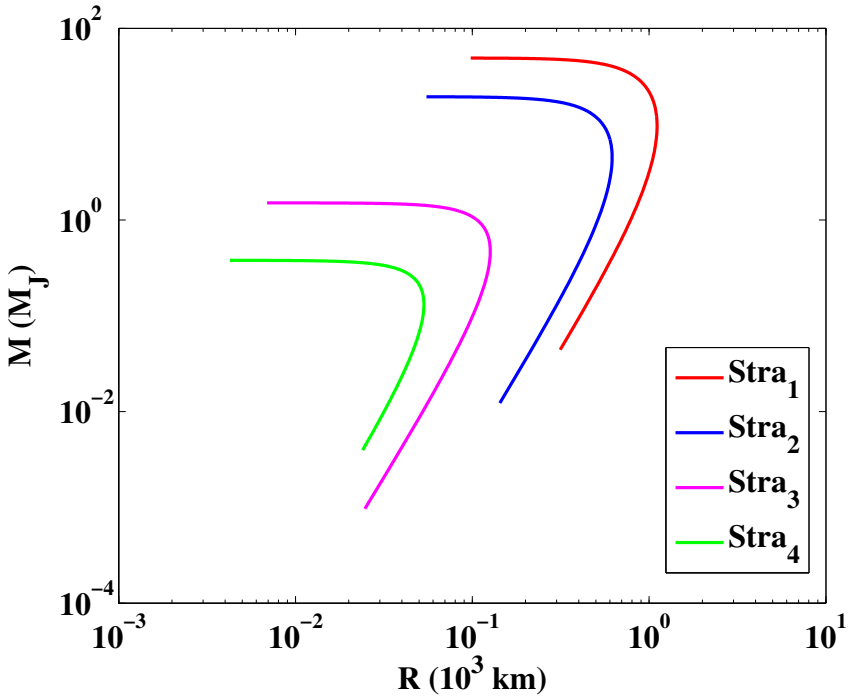


Figure 3.3: Sequence of the strangelet crystal planets for different strangelets from Table 2.3.

We are interested in the macroscopic properties of the planets, namely mass and radii. This is possible from the solution of TOV's equations of general relativity and the EOS given by Eqs (3.10)-(3.11). This system of differential equations is numerically integrated for a given central energy density $\epsilon_c$ from $r = 0$ to $r = R$, where the pressure vanishes, $P(R) = 0$, which defines the planet's surface. Hence, we obtain the radius $R$ and the gravitational mass $M$ of the planet. The family of strangelet crystal planets is shown in Figure 3.3 which shows the gravitational mass as a function of radius until each family reaches the maximum mass. Each point in that figure is a unique planet structure with a particular mass and radius. Given the planet's low mass and their planetary nature, the mass is given in Jupiter's mass units. The results of that figure show that, as expected, a stiffer EOS leads to planetary sequences with higher maximum mass. On the other hand, lower-mass planets associated with smaller central densities, the mass is proportional to $R^3$, which typical for planetary objects because they are mostly composed of incompressible matter. An interesting result is that, as we had mentioned, contrary to what one would expect, crystal planets made of

heavier strangelets lead to a lower maximum mass for planets. Furthermore, for a given mass, planets made of lighter strangelets are larger, which is expected. The reason for such behavior has already been discussed: heavier strangelets have a smaller $Z/A$ ratio, thus they have a less dense electron gas surrounding them, which yields less pressure and hence lower masses. The properties for the maximum-mass of the strangelet crystal planets families found in our study are shown in Table 3.3.2.

Table 3.1: Properties of maximum mass strangelet crystal planets for each strangelet studied. $M_J$ is Jupiter's mass ($M_J \sim 10^{-3} M_\odot$). $\bar{\epsilon}$ is the average density, $r_{td}$ is the tidal disruption, $P_{orb}$ is the orbital period and, $h$ is the gravitational waves' amplitude (see the next section).

| Stra | $M_{max}(M_J)$ | $R(km)$ | $\bar{\epsilon}$ $(g/cm^3)$ | $r_{td}$ (cm) | $P_{orb}$ (ms) | $h$ |
|---|---|---|---|---|---|---|
| 1 | 48.88 | 98 | $2.4 \times 10^{10}$ | $3.9 \times 10^{7}$ | 110 | $3.0 \times 10^{-21}$ |
| 2 | 19.29 | 55 | $5.3 \times 10^{10}$ | $2.9 \times 10^{7}$ | 73.9 | $1.5 \times 10^{-21}$ |
| 3 | 1.51 | 6.9 | $2.1 \times 10^{12}$ | $8.6 \times 10^{6}$ | 11.7 | $4.2 \times 10^{-22}$ |
| 4 | 0.38 | 4.25 | $2.2 \times 10^{12}$ | $8.4 \times 10^{6}$ | 11.3 | $1.1 \times 10^{-22}$ |

## 3.4 Orbital Properties of Strangelet Crystal Planets

Here, we follow in the footsteps of Huang and Yu (2017) and Geng et al. (2015) and determine the relevant properties associated with strangelet crystal planets. The first possibility that we explore is the orbit of exoplanets. Since strange planets are more compact, they can survive in closer orbits, where traditional hadronic planets would be subject to tidal disruptions. When a planet orbits around its host star, the tidal force tends to tear the planet apart, but it can be resisted by the self-gravity of the planet when the two objects are far from each other (Gu et al., 2003). The critical distance, i.e., the so-called tidal disruption radius ($r_{td}$) at which the tidal force[6] is exactly balanced by the self-gravity of

[6]Tidal force, by technical definition, is the differential force of gravity which arises because the force exerted on one body by another is not constant across the diameter in that the side which is the nearest to the second body is subject to more gravitational force compared to the side farther away. If a body is rigid or the complete opposite – flimsy, tidal forces can tear the body in half.

the planet, is defined as (Hills, 1975)

$$r_{td} \approx \left(\frac{6M_\star}{\pi\bar{\epsilon}}\right)^{1/3}, \tag{3.20}$$

where $M_\star$ is the mass of the central host star and, $\bar{\epsilon}$ is the average density of the planet. If the distance is smaller than $r_{td}$, the tidal force will dominate and the planet will be completely broken up. Eq. (3.20) can be conveniently rewritten, as

$$r_{td} \approx 1.5 \times 10^6 \left(\frac{M_\star}{1.4M}\right)^{1/3} \left(\frac{\bar{\epsilon}}{4 \times 10^{14}\ g\ cm^{-3}}\right)^{-1/3} cm. \tag{3.21}$$

One can also determine the period associated with orbits at the tidal disruption radius. From the Kepler's law[7], the radius and period of the orbit are related by (Huang and Yu, 2017)

$$\frac{r^3}{P_{orb}^2} \approx \frac{GM_\star}{4\pi^2.} \tag{3.22}$$

If we take $\bar{\epsilon} = 30\ g.cm^{-3}$ and $M_\star = 1.4M$ , the tidal disruption and the orbital period will be: $\sim 5.6 \times 10^{10}\ cm$ and $\sim 6100\ s$, respectively. On the other hand, for strange planets, with typical densities $\sim 4 \times 10^{14}\ g.cm^{-3}$, we will have $\sim 1.5 \times 10^6\ cm$ as well as ultra-short period $P_{orb} \sim 0.845\ ms$. These results show us a possible way to identify SQM planets: if the tidal disruption and orbital period is significantly less than $\sim 5.6 \times 10^{10}\ cm$ and $\sim 6100\ s$, respectively, so it must be a strange planet (Huang and Yu, 2017).

We can apply this analyses to our model. The results are shown in Table 3.3.2 where we have obtained the tidal disruption, $r_{td}$, and the orbital period, $P_{orb}$, from Eqs. (3.21) and (3.22), respectively, using $M_\star = 1.4M$ . In the table, $M$ is the total mass of the planet, $R$ is the radius, $\bar{\epsilon} = mass/volume$ is the average density, $r_{td}$ is the tidal disruption radius, and $P_{orb}$ is the orbital period. We note that the tidal disruption and the rotation periods of these planets are, as expected, much smaller than those of ordinary planets ($5.6 \times 10^{10}\ cm$; $6100\ s$). In addition, we see that their densities are much higher when compared to ordinary planets ($\sim 1 - 30\ gcm^{-3}$).

Another analysis that we can do here is as follows: according to general relativity, the orbital motion of a binary system can lead to gravitational waves (GW) emission and spiral-in of the system. Geng et al. (2015) showed that

[7] More specifically, here we refer to Kepler's third law.

due to extreme compactness, strange planets can spiral very close to their host compact stars without being tidally disrupted. These systems could potentially serve as a new source for gravitational waves. GW emission from these events happening in our local universe may potentially be strong enough to be detected by upcoming detectors such as Advanced LIGO (aLIGO) (Acernese et al., 2006; Abbott et al., 2016) and the future Einstein Telescope (Hild et al., 2008; Punturo et al., 2010)[8]. This analysis can thus be used as possible evidence for the existence of SQM. In contrast to normal matter planets moving around a compact star, their GW signals are negligibly small since the planet cannot get very close to the central star due to the tidal disruption effect. Following Geng et al. (2015), the strain amplitude of GW from a strange matter system[9], at the last stage of the inspiraling (i.e., when the planet approaches the tidal disruption radius) and at distance $d$ from us, is

$$h = l\left(\frac{M_\star}{1.4M}\right)^{2/3}\left(\frac{\bar{\epsilon}}{4\times10^{14}\ g\ cm^{-3}}\right)^{4/3}\left(\frac{R}{10^4\ cm}\right)^{3}\left(\frac{d}{10\ kpc}\right)^{-1} \tag{3.23}$$

where $l = 1.4\times10^{-24}$, $d$ (in kpc) is the distance of the binary to us, and $R$ is the radius of the star (in cm). If $r_{td}$ is too large, the GW emission will be very weak. For example, at $d = 10\ kpc$, for a typical planet with $M = 5\times10^{-4}M_{Jup}$, $\bar{\epsilon}\sim 10\ g.cm^{-3}$ and, $R\sim 3.6\times10^8\ cm$; disrupted at $5.1\times10^{10}\ cm$, the maximum GW amplitude is only $h\approx 4.9\times10^{-29}$, screen for high density $\sim 30\ g.cm^{-3}$, the GW amplitude is $h\approx 7.05\times10^{-26}$, which is too weak to be detected. For strange planets, however, the strain amplitudes of $GWs$ are between $h\sim10^{-23}-10^{-22}$, at a distance of $d\sim 10\ kpc$ (Geng et al., 2015).

Now employing Eq. (3.23) to strangelet crystal planets, we obtain the results shown in Table 3.3.2. From this table it is clear that a binary system with strangelet crystal planets can emit GW with amplitudes of the order of $\sim 10^{-22}-10^{-21}$ with GW frequencies ($= 2/P_{orb}$) between $18-177$ Hz. These frequency values are within in the most sensitive range of GW detectors like Advance LIGO and the Einstein Telescope (Geng et al., 2015).

[8]The Advanced LIGO (Laser Interferometer Gravitational-Wave Observatory) detectors will be able to see inspiraling binaries made up of two $1.4M$ neutron stars to a distance of 300 Mpc. This horizon distance would even be pushed to 3 Mpc by the future Einstein Telescope.

[9]Indeed, the measurable signals of GWs are the amplitudes of two polarized components ($h_+$ and $h_-$), for merging binaries, we assume the waves to be sinusoidal and define an effective strain amplitude $h$, after averaging over the orbital period (Geng et al., 2015)

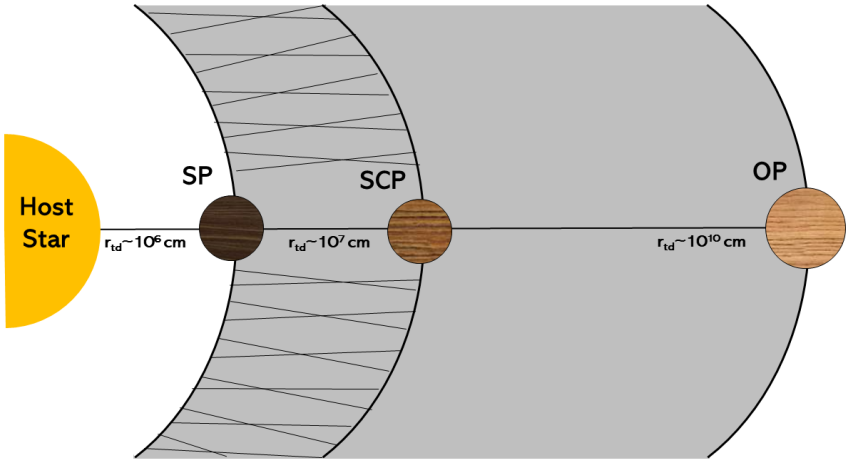


Figure 3.4: Diagram representing different orbital properties between strange planets (SP), strangelet crystal planets (SCP), and ordinary planets (OP). The dashed area indicate possible orbital region only for SP, gray area for SP and SCP and the region beyond for OP. $r_{td}$ is tidal disruption radius (and their orders of magnitude for each model). In this picture, we can see that SCPs exhibit intermediate properties between SPs and OPs. [The distances are not in scale.]

Finally, we can summarize the properties of strange crystal planets (SCP) and compare them with the ordinary planets (OP) and strange planets (SP). In the Fig. 3.4, we see schematically the difference between them. The hashed area indicate orbits that can only be explained by SPs. The gray area represents orbits that can be explained by SPs and SCPs. As for the region beyond the ordinary planet orbit, one cannot distinguish between models. These differences are summarized in the Table 3.4, we see that our model differs from other cases in which: they have higher $r_{td}$ and $P_{orb}$ compared to strange planets, and lower $r_{td}$ and $P_{orb}$ compared to ordinary planets. Besides, strangelet crystal planets and strange planets have the strain amplitude in the same order, whereas, ordinary planets have a much lower strain amplitudes than the other SQM objects.

Table 3.2: Comparisons: strangelet crystal planets vs ordinary planets and strange planets.

| Object Planets | $\bar{\epsilon}$ $(g/cm^3)$ | $r_{td}$ $(cm)$ | $P_{orb}$ $(s)$ | $h$ |
|---|---|---|---|---|
| Ordinary Planets | | | | |
| Low density | $\sim 10$ | $5.1 \times 10^{10}$ | $\sim 5263$ | $4.9 \times 10^{-29}$ |
| High density | $\sim 30$ | $5.6 \times 10^{10}$ | $\sim 6100$ | $7.1 \times 10^{-26}$ |
| Strangelet Crystal Planets | $\sim 10^{10} - 10^{12}$ | $\sim 8 \times 10^{6} - 4 \times 10^{7}$ | . 0.110 | $\sim 10^{-22} - 10^{-21}$ |
| Strange Planets | $\sim 4.0 \times 10^{14}$ | $\sim 1.5 \times 10^{6}$ | $\sim 8.45 \times 10^{-4}$ | $\sim 10^{-23} - 10^{-21}$ |

## 3.5 Application to Sub-stellar Objects

Since our objects have masses within $\sim 10^{-3} - 50 M_J$ ($\sim 10^{-6} - 0.05 M$ ) and, crystalline internal structure, then we can use it as a possible application to some sub-stellar objects such as Brown Dwarfs (BD), Exoplanets, dwarf planets. According to Burgasser (2009), Brown dwarfs ("failed" stars) are "stellar" objects with insufficient mass to sustain core hydrogen fusion reactions. The mass limit for sustained hydrogen fusion is roughly $\sim 75 - 90\ M_J$ (Chabrier and Baraffe, 2000). This mass limit establishes a formal division between stars (or very low mass stars (Auddy et al., 2016)) and brown dwarfs. Following the mass regime, the distinction between giant planets (such as Jupiter) and brown dwarfs is that objects between $\sim 12 - 90 M_J$, are arbitrarily designated as brown dwarfs (Burrows and Liebert, 1993). The possible dividing line limit between brown dwarfs and planets is $\sim 12 M_J$, thus objects with masses less than this are considered planets (Basri and Brown, 2006). On the other hand, an exoplanets is an object orbiting a star host like our sun (Basri and Brown, 2006). Finally, due to spherical format and lower masses for strangelets crystal planets made of strangelets$_4$, these objects could be considered into the dwarf planets ($\sim 10^{-4} M_J$) category according to International Astronomical Union (IAU) (Sarma et al., 2008; Brown and Schaller, 2007). Thus, in this sense our objects called strangelet crystal planets could be regarded as possible theoretical models for brown dwarfs, exoplanet and dwarf planets studies with comparable masses.

## 3.6 Summary

In this chapter, we have proposed a novel planet-like configuration: Strangelet crystal planets (Zapata and Negreiros, 2020). These objects are low-pressure, made up of strangelets arranged in periodic crystals (Glendenning, 2012; Heiselberg, 1993). This model differs from previously proposed strange star models (Alcock et al., 1986; Glendenning et al., 1995; Kettner et al., 1995; Alcock and Olinto, 1988) in that in those models SQM is found in bulk and possibly crusted by ordinary hadronic matter. Here we have followed the approach of Alford et al. (2012) and Jaikumar et al. (2006) in which SQM takes a crystalline form. Within such scenario, self-bound strangelets can organize themselves in a crystal lattice, permeated by electron gas (needed for charge neutrality); such matter could then form self-gravitating objects supported against gravitational pull by the electronic pressure, much like the white dwarfs do (Glendenning, 2012). We have determined the masses and radii of such objects, and we found that their mass remind us objects like brown dwarfs and exoplanets or ordinary planets, but with slightly smaller radii than ordinary sub-stellar objects. Furthermore, we have calculated possible observable signatures of such a model using the concept of tidal disruption radius and amplitude of GWs that could be emitted by such systems. As expected, we have found that due to their compactness, the tidal disruption radii of strangelet crystal planets are significantly smaller than those of ordinary planets. We have found, however, that when compared to previously proposed strange planet models, our scenario leads to higher tidal disruption radii. This means that strangelet crystal planets exhibit an intermediate behavior, with possible orbital properties not as extreme as those of strange planets but not as mild as those of ordinary planets.

Chapter 4

# Strange Quark Stars

## 4.1 Introduction

In this chapter, we assume the strange quark matter (SQM) hypothesis (Bodmer, 1971; Witten, 1984; Terazawa, 1979) and we explore the cooling of isolated quark stars (QS). These objects are composed of a quark matter core and crusted by matter. We adopt two kinds of crust for the star's core: (i) a crust made of purely nuclear matter following the Baym-Pethick-Sutherland (BPS) equation of state (Baym et al., 1971) and, (ii) a crust made of nuggets of strange quark matter, i.e. strangelets as described by Jaikumar et al. (2006). Both theoretical models have the same quark matter core according to the MIT bag model equation of state (EoS) (Farhi and Jaffe, 1984; Chodos et al., 1974b,a; Weber et al., 2009). Our main purpose is to quantify the effects of strangelets crust matter on the cooling calculation and relaxation times of theses strange stars (Zapata, J. et al., 2022). We also include the possible color superconductivity effect in the quark core. Finally, the numerical results are compared with the recently observed data found in Potekhin et al. (2020). we have found that objects with a strangelet crust have a significantly different thermal behavior.

As Chapter 3, we take into account the strange quark matter (SQM) hypothesis (Bodmer, 1971; Witten, 1984; Terazawa, 1979) and consider compact stars that are made up of absolutely stable strange matter. If the SQM hypothesis is true, the strange stars would be a new class of astronomical compact objects (Witten, 1984; Alcock et al., 1986; Weber, 2005; Baym and Chin, 1976; Haensel et al., 1986b). Relevant to the work we present in this chapter is the

research of Alcock et al. (1986), in which they considered the possibility for a strange star to maintain a thin crust of normal matter. They pointed out that the crust was mainly influenced by two factors: (i) the tunnel effect through which ions might penetrate the core-crust gap and, (ii) that the density at the base of the crust can not be denser than the neutron drip ($\epsilon_{drip}$) since free neutrons would come out of nuclei and fall into the strange core (Alcock et al., 1986; Glendenning et al., 1995; Glendenning and Weber, 1992). The latter consideration was revised by Huang and Lu (1997) where they found that the maximum density at the base of the crust is about $\sim \epsilon_{drip}/5$ giving a maximum mass of $\sim 3.4 \times 10^{-6} M$ for the crust, which is about one order of magnitude smaller than what had been found before. In the traditional picture, the surface of a bare strange star has a sharp edge of thickness $\sim 1$ fm (Alcock et al., 1986). Below the surface lies quark matter which on the outermost layer should be positively charged (due to exhaustion of massive strange quarks), and above which resides a cloud of electrons (that guarantees the star's charge neutrality) (Alcock et al., 1986; Stejner and Madsen, 2005; Usov, 1997). It has been shown, however, that if the surface tension $\sigma$ of the interface between quark matter and the vacuum is less than a critical value, $\sigma_{crit}$ then large lumps of strange matter become unstable against fission into smaller pieces (Jaikumar et al., 2006; Alford et al., 2006). As a result, the lower density surface region is replaced by a "mixed-phase" involving nuggets (strangelets) of positively charged strange matter in a neutralizing background of electrons. Jaikumar et al. (2006), assuming zero surface tension and neglecting Debye screening, estimated that the "mixed-phase" crust might be $40 - 100$ m thick. Later, Alford and Eby (2008) found that if the surface tension of quark matter is low enough, the surface of a strange star will be a crust consisting of a crystal of charged strangelets in a neutralizing background of electrons. They calculated the thickness of the crust, taking into account the effects of surface tension and Debye screening of electric charges. Their results showed that the strangelet crust's size can range from zero to hundreds of meters and, the thickness is greater when the strange quark is heavier and the surface tension is smaller (Alford and Eby, 2008). In this work, we will further explore the possibility of a strangelet crust on strange stars and their implications to the thermal evolution of such stars.

Since the proposal of strange stars, many efforts have been devoted to indicate observational properties (if any) that may be useful to distinguish strange stars from neutron stars, as they share many similar (observable) macroscopic properties (such as gravitational mass, for instance). One possibility to reach that goal is by their thermal evolution, as quark stars may exhibit a fairly distinct cooling as opposed to ordinary neutron stars. The cooling of neutron stars is dominated, mainly, by neutrino emissions for the initial $\sim 1000$ years, later being replaced by surface photon emissions (Page et al., 2006; Tsuruta, 1998). Due to very different compositions/morphology between the neutron star core and crust, it takes $\sim 1 - 100$ years for the star to thermalize[1] (Lattimer et al., 1994; Sales et al., 2020).

The situation for crusted strange stars is significantly different, since the presence of unconfined quark matter plays an important role in the cooling of the star (Blaschke et al., 2000; Grigorian et al., 2005). In this chapter, we will revisit the cooling of strange quark stars, considering the effects of a strangelets crust as described by Jaikumar et al. (2006). We will compare our findings to the cooling of quark stars (QS) with nuclear matter crusts. Our main goal is to quantify the effects of a strangelet crust on the cooling calculation of quark stars. We will also study the thermal relaxation[2] of quark stars, which to the extent of our knowledge has never been studied in details, therefore we study such properties here.

We proceed as follows: first, we will describe the microscopic model for crusted strange stars, and we present the results for the macroscopic structure of our two models of quark stars. Second, we will explore the thermal behavior of these stars and analyze the thermal relaxation times as well. Furthermore, we also include superconductivity effect and compare them with the current observations.

[1] Thermalisation is the process of physical bodies reaching thermal equilibrium through mutual interaction.

[2] This is a typical time for the cooling wave to reach the star's surface.

## 4.2 Microscopic Model

### 4.2.1 The Equation of State: Core + Crust

We assume that the quark stars crust matter is a crystal lattice of a single species of atomic nucleus $(A, Z)$ (or strangelets) embedded in an electron gas. For comparison reasons, we adopt two kinds of crust for the star's core: (i) a crust made of purely nuclear matter following the Baym-Pethick-Sutherland (BPS) equation of state and, (ii) a strangelets crust. The traditional nuclear matter is the Baym, Pethick, and Sutherland ($BPS$) equation of state (Baym et al., 1971), in which case the crust must necessarily have a maximum density limited by neutron drip density ($\epsilon_{drip} \sim 4 \times 10^{11}\ g\ cm^{-3}$). The most significant aspect of this density domain is that it consists of a Coulomb lattice of heavy ions immersed in an electron gas. The heavy ions become ever more neutron rich as the neutron drip density is approached from below (see Baym et al. (1971) for more details). On the other hand, we use the EOS for strangelets crust as described in chapter 2, section 2.4. That is, if the surface tension of the interface between quark matter and the vacuum is less than a critical value, then large lumps of strange matter become unstable against fission into smaller pieces; as a result the crust consists of a crystalline structure of charged spherical strangelets in a neutralizing background of electrons. In this picture, electrons contribute to the pressure while strangelets contribute to the energy density. Finally, we adopt the strange quark matter equation of state to the core of the quark star as shown in chapter 2, section 2.5. The parameters are set as $m_s = 100\ MeV$, $B^{1/4} = 128.9\ MeV$ and $\alpha_s = 0.4$ (the strong interaction coupling constant)[3].

Hence, the structure of strange stars (core + crust) model for strange quark stars here is schematically illustrated in Figure 4.1, where we have the cross–section of a strange star. The equation of state should consist of two parts: core and crust. The core matter follows the MIT bag model (see section 2.5), involved by a crust matter (pure nuclear matter or strangelets). The Figure 4.2 shows the equation of state of a quark star with a nuclear (BPS) matter ("BPS" labelled) and strangelets crust ("Strangelets" labelled). The transition point between core and crust occurs at $\epsilon_{tr} \sim 153.76\ MeV.fm^{-3} \sim 2.74 \times 10^{14} g\ cm^{-3}$.

[3] $\alpha_s$ has a little effect on the equation of state, which remains largely unaltered for different values of this constant (Negreiros, 2009).

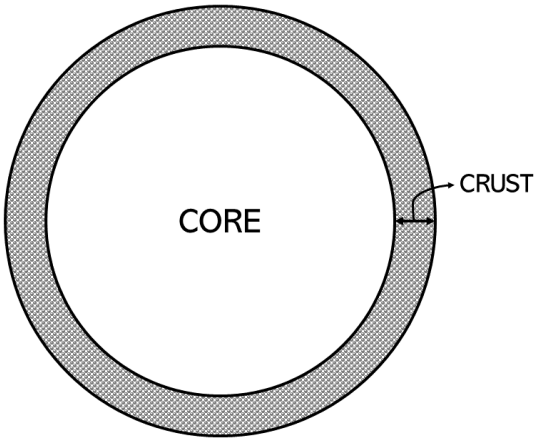


Figure 4.1: Cross–section of a strange star (core + crust) model used in this work. The star's core consists of pure 3-flavor strange quark matter following the MIT bag model, and the crust consists of a pure low-density nuclear matter (or strangelets).

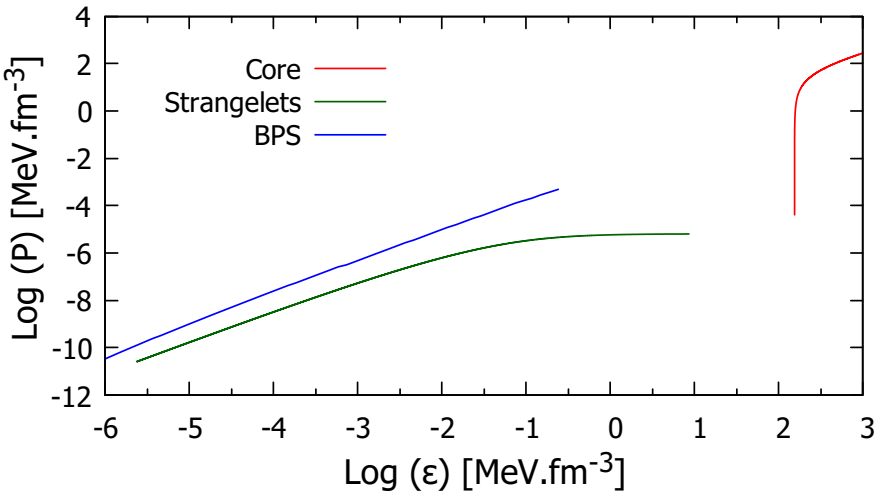


Figure 4.2: Equation of state for strange quark matter (SQM) surrounded by (i) a nuclear BPS crust and (ii) a Strangelets crust.

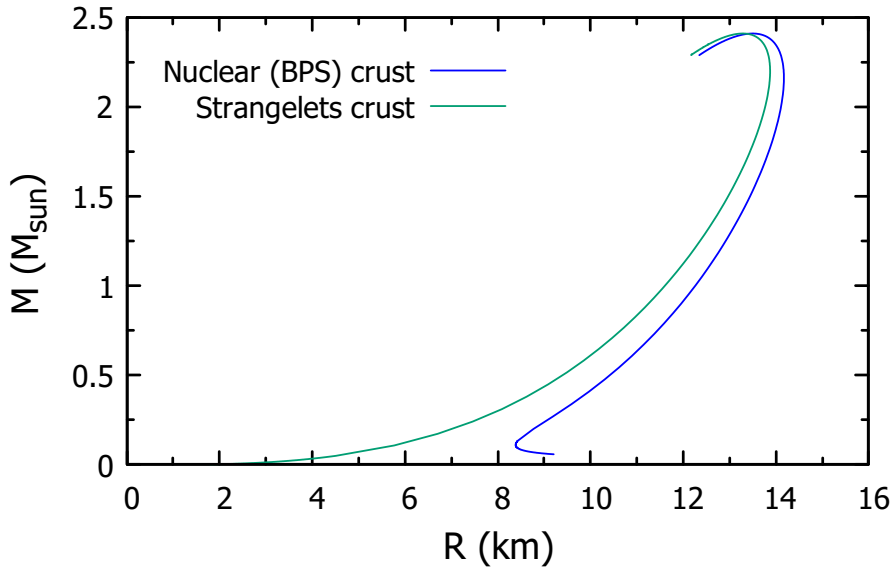


Figure 4.3: Mass-radius diagram for quark stars, whose equations of state are shown in Fig. 4.2. Both sequences have the same maximum mass $\sim 2.41M$

### 4.2.2 Structure of Quark Stars

With the EOS in Figure 4.2, we can solve the Tolman-Oppenheimer-Volkoff[4] (TOV) equation (Oppenheimer and Volkoff, 1939; Tolman, 1939) and find the structure of the quark stars. In Figure 4.3 we show the sequences of quark stars obtained from EOSs. We note that, as expected, the only difference between the models studied is the description of the crust, both sequences have the same maximum mass $\sim 2.41M$ . Furthermore, due to the different crust modelling, we also see a significant difference between the stellar radius in each sequence.

We summarize the macroscopic properties found for the two models studied in Table 4.1. The most notable distinction between them can be found as: quark stars with nuclear BPS matter crust have larger radii, crust thickness and mass crust: $\Delta R_{crust} \sim 500\ m$, $\sim 10^{-4}M$ , respectively. Quark stars with strangelets crust, on another hand, have smaller radii, crust thickness and crust mass: $\Delta R_{crust} \sim 20\ m$ and $\sim 10^{-5}M$ , respectively. At this point, our results from Table 4.1 are in agreement with recent observational measures and estimates. We have found that they are within the latest estimates from *Neutron Star Interior Composition Explore* (NICER) data.

[4]See Appendix D

For instance, the observed gravitational mass and radius of isolated millisecond pulsar PSR J0030+0451 are estimated to be $1.34^{+0.15}_{-0.16}M$ and $12.71^{+1.14}_{-1.19}$ km, respectively (Riley et al., 2019; Miller et al., 2019). Also, with the pulsars PSR J1614-2230, with $M = 1.97 \pm 0.04M$ (Demorest et al., 2010), and PSR J0348+0432, with $M = 2.01 \pm 0.04M$ (Antoniadis et al., 2013); which could be explained by the model we employed in our analysis.

Table 4.1: Properties of some quark stars from Fig. 4.3. We differentiate them with the label strangelets or nuclear (BPS) crusts.

| $\epsilon_c$ | M | Strangelets crusts | Nuclear (BPS) crusts |
|---|---|---|---|
| $(MeV/fm^3)$ | $(M\ )$ | R (km) | R(km) |
| 237.24 | 1.42 | 12.78 | 13.27 |
| 257.49 | 1.60 | 13.19 | 13.62 |
| 288.59 | 1.82 | 13.55 | 13.93 |
| 327.36 | 2.00 | 13.77 | 14.11 |

## 4.3 Cooling on Quark Stars

### 4.3.1 Thermal Evolution Equations

The following cooling calculation are performed for spherically symmetric, non–rotating stars models, which are constructed in the framework for general relativity theory. The cooling of a compact star is governed by the general relativistic thermal energy balance and transport equations given[5] by ($G = c = 1$) (Weber, 2017; Thorne, 1977; Van Riper, 1991)

$$\frac{\partial(l(r,t)e^{2\Phi(r)})}{\partial m} = -\frac{1}{\epsilon\sqrt{1-2m(r)/r}}\left(\epsilon_\nu(r,T)e^{2\Phi(r)} + c_v(r,T)\frac{\partial(T(r,t)e^{\Phi(r)})}{\partial t}\right) \tag{4.1}$$

$$\frac{\partial(T(r,t)e^{\Phi(r)})}{\partial m} = -\frac{(l(r,t)e^{\Phi(r)})}{16\pi^2 r^4 \kappa(r,T)\epsilon(r)\sqrt{1-2m(r)/r}}, \tag{4.2}$$

[5] See Appendix D

where the macroscopic dependencies are: the radial distance $r$, the energy density $\epsilon(r)$ and, the stellar mass $m(r)$. Moreover, the thermal properties are represented by the temperature $T(r,t)$, luminosity $l(r,t)$, neutrino emissivity[6] $\epsilon_\nu(r,T)$, thermal conductivity $\kappa(r,T)$ and, specific heat $c_v(r,t)$.

The boundary conditions of Eqs. (4.1) and (4.2) are determined both by the luminosity at the stellar center

$$L(r=0)=0, \tag{4.3}$$

this means that there is no heat flux at the center of the star, and at the stellar surface

$$T(r=R)=T_s, \tag{4.4}$$

this is, the luminosity is defined by the relationship between the mantel temperature and the temperature outside the star (Page et al., 2006; Blaschke et al., 2000) (see appendix D). These equations need to be solved numerically. Since the central star temperature at the beginning of its life is not larger than $10^{11}\ K \sim 1\ MeV$ (Weber, 2017), the effects of finite temperatures on the equation of state can be relegated to a very good approximation. Consequently, TOV's equations do not depend on time and thus need to be solved only once - which is fortunate as the thermal and structural properties are then uncoupled (Weber, 2017). Now, we will discuss the microphysical processes for the cooling equations of quark stars.

### 4.3.2 Microphysical Processes

The microphysical properties of quark stars are analogous to those of neutron stars, except in this case they involve quarks rather than baryons. Additionally, the thickness of the crust of quark stars will have a strong impact on the cooling of those objects, as we will see later.

[6]Neutrino emissivity is a quantity that quantifies the amount of energy emitted per unit volume per unit time at a given position within the star. It is the kinetic energy of neutrinos and antineutrinos produced by a certain type of reaction, such as beta decay.

### Core

Neutrino emission is the main mechanism driving the cooling of quark stars. Due to the distinct composition of the core and the crust, we have different neutrino emission processes. The core's neutrino emissivity can be written as

$$\epsilon_{\nu}^{core} = \epsilon_{\nu,DU} + \epsilon_{\nu,MU} + \epsilon_{\nu,BR}. \tag{4.5}$$

The sub-indices DU stands for direct Urca, MU for modified Urca and BR for Bremsstrahlung, processes.

**The direct Urca process** in quark stars involve quarks. These processes are given by

$$d \to u + e^{-} + \bar{\nu_e}, \tag{4.6}$$

$$u + e^{-} \to d + \bar{\nu_e}. \tag{4.7}$$

The emissivity of such process was calculated in Iwamoto (1982) and it is given by

$$\epsilon_{\nu,DU} = 8.8 \times 10^{26} \alpha_c \left(\frac{\rho_b}{\rho_0}\right) Y_e^{1/3} T_9^6 \; erg \; cm^{-3} \; s^{-1}, \tag{4.8}$$

where $\alpha_c$ is the strong coupling constant, $\rho_b$ is the baryon number density, $\rho_0 = 0.16 \; fm^{-3}$ is the nuclear matter density, $Y_e = \rho_e/\rho$ is the number of electron per baryon, and $T_9$ is the temperature in units of $10^9$ K (that is, $T_9 = T/10^9$ K). The direct Urca process will only take place if the triangle inequalities (and cyclic permutations of it) are satisfied, that is,

$$k_{F_i} + k_{F_j} \geq k_{F_e}, \tag{4.9}$$

where $k_{F_e}$ is the fermi momentum of the electron, and $k_{F_{i,j}}$ is the fermi momentum of quark (just like in neutron stars), in this case however, due to the high abundance of quarks this condition is more easily achieved. In general, as long as electrons are present, the direct Urca process will take place in quark stars.

**The modified Urca process** is similar to the direct Urca except for the presence of a bystander particle $q$ whose function is to guarantee the conservation of momentum. This process is represented by the following reaction

$$q + d \to u + q + e^{-} + \bar{\nu_e}. \tag{4.10}$$

The emissivity associated with this process is given in Iwamoto (1982); Negreiros (2009) by

$$\epsilon_{\nu,MU} = 2.83 \times 10^{19} \alpha_c^2 \left(\frac{\rho_b}{\rho_0}\right) T_9^8 \; erg \; cm^{-3} \; s^{-1}. \tag{4.11}$$

As before, $\alpha_c$ is the strong coupling constant, $\rho_b$ is the baryon number density, $\rho_0 = 0.16 \; fm^{-3}$ is the nuclear matter density, $Y_e = \rho_e/\rho$ is the number of electron per baryon, and $T_9$ is the temperature in units of $10^9$ K. Finally, **the quark Bremsstranhlung**[7] process was calculated in Iwamoto (1982); Negreiros (2009) and is given by

$$\epsilon_{\nu,BR} = 2.98 \times 10^{19} \left(\frac{\rho_b}{\rho_0}\right) T_9^8 \; erg \; cm^{-3} \; s^{-1}. \tag{4.12}$$

**The specific heat** in quark stars is due to the electrons and quarks ($u$, $d$, and $s$)

$$C_v^{core} = C_v^{e^-} + C_v^q, \tag{4.13}$$

These are given respectively (Iwamoto, 1982; Negreiros, 2009)

$$C_v^q = 0.6 \times 10^{20} \left(\frac{Y_e \rho_b}{\rho_0}\right)^{2/3} T_9 \; erg \; cm^{-3} \; K^{-1}, \tag{4.14}$$

$$C_v^{e^-} = \frac{K_B^2}{3\tilde{}^3} T \sqrt{m_{e^-}^2 + k_{e^-}^2}\, k_{e^-}, \tag{4.15}$$

where $K_B$ is the Boltzmann constant and $k_{e^-}$ is the Fermi momentum of the electron.

**The thermal conductivity** of quark stars is given by (Haensel, 1991)

$$\kappa^{core} = 3.4 \times 10^{22} \left(\frac{\alpha_c}{0.2}\right)^{-1/2} T_{10}^{-1} \frac{\rho_b}{\rho_0} \; \frac{erg}{cm \; s \; K}, \tag{4.16}$$

where $T_{10} = T/10^{10}$ K.

[7] *Bremsstranhlung* from *bremsen* "to break" and *Strahlung* "radiation"; i.e., "braking radiation" or "deceleration radiation", is electromagnetic radiation produced by the deceleration of a charged particle when deflected by another charged particle, typically an electron by an atomic nucleus.

### Crust

The quark stars that we are considering have crusts with different composition than the core. The total neutrino emissivity of the crust is given by the sum of the emissivity of each of these three processes

$$\epsilon_{\nu}^{crust} = \epsilon_{\nu,BR} + \epsilon_{\nu,pair} + \epsilon_{\nu,plasma}, \tag{4.17}$$

where $\epsilon_{\nu,BR}$ is the emissivity of electron Bremsstrahlung, $\epsilon_{\nu,pais}$ for $e^{-}e^{+}$ pair annihilation and $\epsilon_{\nu,plasma}$ of plasmon decay.

The **electron Bremsstrahlung**[8] in the crust, that is, the electrons scattering off heavy ions [(A, Z), with a certain atomic number $Z$ and mass number $A$] in the crust will lead to the production of neutrinos. The emissivity of such process has been given in Kaminker et al. (1998) by

$$\epsilon_{\nu,BR} = 10^{x}\ erg\ cm^{-3}\ s^{-1}, \tag{4.18}$$

where

$$\begin{aligned} x = {} & 11.204 + 7.304\tau + 0.2976r - 0.37\tau^2 + 0.188\tau r - 0.103r^2 \\ & + 0.0547\tau^2 r - 6.77 \ln\left(1 + 0.228\frac{\epsilon}{\epsilon_0}\right), \end{aligned} \tag{4.19}$$

and $\tau \equiv \log(T/T^8)$, $r \equiv \ln(\rho_{12})$; and $\epsilon_0 = 2.8 \times 10^{14}\ g\ cm^{-3}$ is the nuclear density.

The **annihilation of $e^{-}e^{+}$ pairs**[9] in the crust also generates neutrinos. The emissivity from this process does not have a simple expression, but just say that

$$\epsilon_{\nu,pair} \propto 10^{23}\ erg\ cm^{-3}\ s^{-1} \tag{4.20}$$

(see Yakovlev et al. (2001) for a detailed description.).

The **plasmon decay**[10] (quantizations of plasma oscillations) formed in the crust of quarks stars produce a pair of neutrinos. We use the following emissivity

[8] $e^{-} + (A, Z) \rightarrow e^{-} + (A, Z) + \nu + \bar{\nu}$.
[9] $e^{-} + e^{+} \rightarrow \nu + \bar{\nu}$.
[10] $\gamma_p \rightarrow \nu + \bar{\nu}$, where $\gamma_p$ represents a quantum of plasma oscillation.

for this process, given by (Yakovlev et al., 2001)

$$\epsilon_{\nu,plasma} = Q_c \frac{C_V^2}{96\pi^4\alpha}\left(\frac{T}{T_r}\right)^9 (16.23 f_p^6 + 4.604 f_p^{7.5}) e^{-f_p}, \tag{4.21}$$

where $Q_c \approx 1.023 \times 10^{23}\ erg\ cm^{-3}\ s^{-1}$ is the electron "Compton neutrino emissivity"; $T_r \equiv m_e c^2/K_B \approx 5.93 \times 10^9$ K is the electron relativistic temperature; and $f_p$ is the electron plasma parameter (Yakovlev et al., 2001; Negreiros, 2009).

On the other hand, we can write **the crust specific heat,** as

$$C_v^{crust} = C_v^e + C_v^n + C_v^i \tag{4.22}$$

It is analogous to the specific heat in the core. Where $C_v^e$ is the specific heat of the electrons given by Eq. (4.15), and $C_v^n$ is the specific heat for the neutrons (just for nuclear BPS crust) given by the baryons specific heat,

$$C_v^b = \frac{K_B^2}{3\tilde{}3} T m_b^\star k_b \tag{4.23}$$

where $m_b^\star$ is the effective mass of the baryon and $k_b$ the baryon Fermi momentum. $C_v^i$ is the specific heat of the ions, and it depends on the properties of the ions found at the crust. These properties are the Fermi momentum, mass number $A$ and atomic number $Z$ (Negreiros, 2009).

The **thermal conductivity** of electrons and neutrons scattering off ions in the crust was calculated in Potekhin et al. (1999)

$$\kappa^{crust} = \frac{\pi^2 K_B^2 T \rho_e}{3\sqrt{m_l^2 + k_l^2}\nu_e} \tag{4.24}$$

where $\nu_e$ is a variable that depends on the ion's properties at the desired density.

This summarizes all the neutrino emissivities, specific heats and thermal conductivities that take place in the core and crust of the quark star studied here for solving the Eqs. (4.1)– (4.2).

### Surface Photon Luminosity

At the late stages of quark star's thermal evolution, the photon luminosity become the most important cooling process. This can be expressed, for the local

observer, as (Negreiros, 2009; Weber, 2017)

$$L_\gamma = 4\pi R^2 \sigma_{SB} T_S^4, \tag{4.25}$$

with $T_S$ is the surface temperature, $\sigma_{SB}$ the Stefan–Boltzmann constant and $R$ the stellar radius. For an observer at infinite must take into account the red-shift: $R_\infty = e^{-\Phi} R$ and $T_\infty = e^{\Phi} T_S$, where $e^{2\Phi} = g_{00}$. Thus, the luminosity observed at infinite is given by

$$L_\infty = 4\pi R_\infty^2 \sigma_{SB} T_\infty^4 . \tag{4.26}$$

We will use the temperature at infinity $T_\infty$ (later as $T_s$) as a main output of the cooling simulations, and we will compare it with observed data.

### 4.3.3 Cooling Results

The previous sections provide us with the description of the different ingredients that enter the modeling of the thermal evolution of our quark star's models. Solving the thermal equations (4.1)- (4.2) with the micro-physical ingredients (last section) we can get the cooling behavior of quark stars. Remembering that, for the quark core, we consider the processes involving quarks: the quark direct Urca (QDU), quark modified Urca (QMU), and quark bremsstrahlung processes (QBM). If the electron fraction vanishes entirely in quark matter ($Y_e = 0$, in the limit in which $m_s \to 0$), both the quark direct and the quark modified Urca processes become unimportant, and the neutrino emission is then dominated by bremsstrahlung processes only. The emissivities of such processes were calculated in Eq. (4.5), we use the specific heat for the quark phase as calculated in Eq. (4.14) (and Eq. (4.15) for electrons as well) and, the thermal conductivity comes from Eq. (4.16). At the crust (both strangelet and nuclear) we consider all expected thermodynamical processes with thermal conductivity dominated by the electrons and specific heat connected to $(A, Z)$ of the nuclei (or strangelets). The equations of the thermal processes taking place in the crust are (4.17)- (4.24).

To investigate the difference between a quark star with nuclear (BPS) crust and quark stars with strangelets crust, we analyze the cooling behavior of quark stars of the same gravitational mass for both models. The thermal evolution is illustrated in Figure 4.4, where we show a typical cooling curve, that is, the red-shifted surface temperature ($T_s$) as a function of the age ($t$) of the star. In this figure, solid lines represent quark stars with nuclear (BPS) crust, and dashed lines

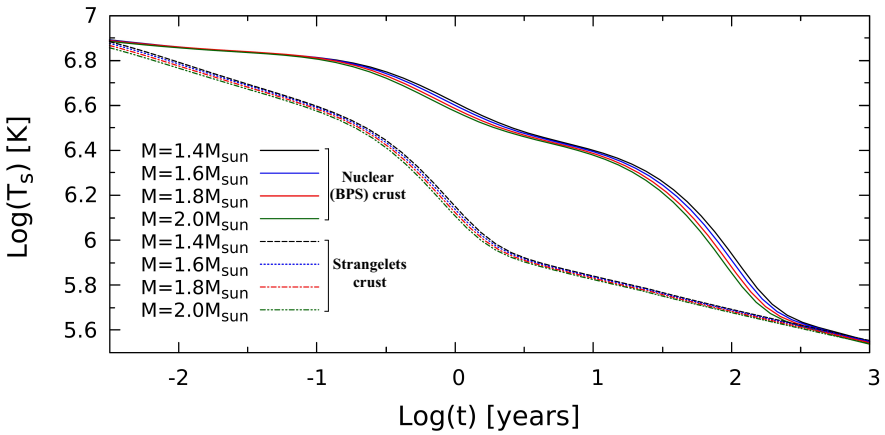


Figure 4.4: Cooling curves of quark stars with gravitational masses from Table 4.1. $T_s$ denotes the red-shifted temperature and the x-axis the age $t$. Solid lines represent quark stars with nuclear (BPS) crusts, and dashed lines are stars with strangelets crusts. Superfluidity is neglected here.

are stars with strangelets crust. In this first moment, superfluidity is neglected. The results indicate that there is little difference between the cooling of stars with different gravitational mass within the same model, both for stars with nuclear (BPS) crust and for stars with strangelets crust. Additionally, for each model, as the star's mass increases then, the surface temperature is slightly lower. This behavior is maintained in the next sections for different gravitational masses. On the other hand, we can notice a significant difference when comparing the cooling behavior exhibited in each model. Most noticeably, quark stars with strangelets crust cool down significantly faster than quark stars with nuclear (BPS) crust. We believe that is due to the thinner nature of the strangelets crust. Next, we talk about the thermal relaxation process suffered by stars due to the difference in the nature of the matter present in the crust and in the core and the different behavior of neutrino emissivity, specific heat, and conductivity in these two regions of the star.

### 4.3.4 Thermal Relaxation

As we have mentioned, the DU neutrino emissivity, i.e. the loss of thermal energy due to neutrino escape, is much more intense in regions with estimated densities of $2-3$ times the nuclear saturation density (see Eq.(4.8)). As a consequence, the temperature of this region reaches a value much lower than that of the upper part

of it. Due to the difference in the intensity of the neutrino emissivity between the crust and the core of the star, two temperature gradients are established inside the star: one between the crust and the upper part of the core, and a more intense one between the latter and the region where the DU process is active. During the first moments of cooling, the temperature gradient between the central region with the DU process and the upper part of it, establishes a flow of heat from the latter to the former, as a kind of "cold wave" propagates from the top of the central region towards the surface. Soon, this wave reaches the base of the crust and the star's core thermalizes, in addition to the already existing temperature gradient between the core and the crust being accentuated. After these first moments of thermal evolution, the cold wave propagates through the crust and, when it reaches the surface, the surface temperature of the star drops abruptly, causing these two regions to thermalize, and the star to become isothermal. Therefore, the time this cold wave reaches the surface of the star is defined as the thermal relaxation time.

In order to quantify the faster cooling exhibited by quark stars with strangelets crust, we now discuss their thermal relaxation. As shown by Lattimer et al. (1994), the thermal relaxation $t_w$ is defined as the moment of the most negative slope of the cooling curve of a young neutron star. It is given in Gnedin et al. (2001) by

$$t_w = max \left| \frac{dln(T_s)}{d(ln(t))} \right| . \tag{4.27}$$

For ordinary neutron stars, such relaxation times are typically between $\sim 10-100$ years. The thermal relaxation time for ordinary neutron stars is determined mainly by the crust thickness $\Delta R_{crust}$ (Lattimer et al., 1994; Gnedin et al., 2001). Although it has been recently demonstrated that depending on how widespread (within the core of the star) the direct Urca process, at such times may be drastically larger (Sales et al., 2020). To the extent of our knowledge, the relaxation time of quark stars has never been studied in detail, therefore we consider such propertied here. In Figure 4.5 we show the $\ln(T_s)$ variation rate with respect to $\ln(t)$ for a representative sample of quark stars of our two models. Solid lines represent the quark stars with nuclear (BPS) crust, and dashed lines are those with strangelets crust. Diamonds and stars indicate the maximum absolute value of each curve, thus representing the relaxation time. We now have a quantitative measure of how fast quark stars with strangelets crust cool down with respect to those with BPS crust. We perceive that the

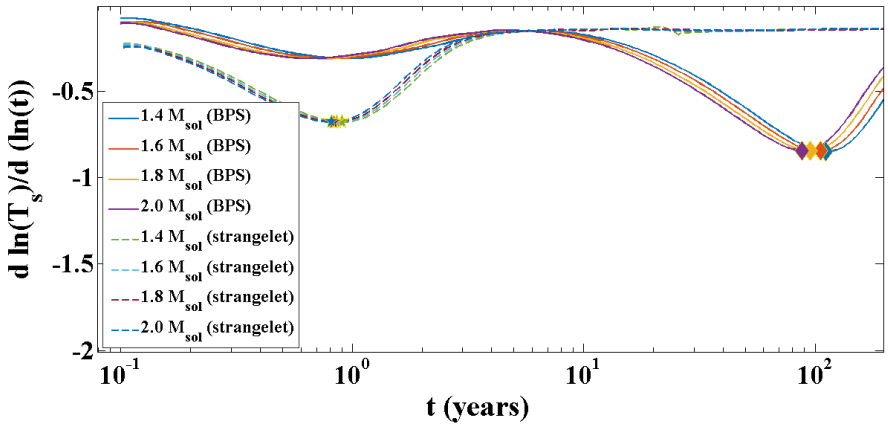


Figure 4.5: The $\ln T_s$ variation rate with respect to $\ln t$ versus ages for our quark stars from Fig. 4.4. Solid lines are quark stars BPS crusted, and dashed lines are strangelets crusted. The highlighted diamond and star points represent the moment of the most negative slope, i.e, their relaxation times.

relaxation times of quark stars with strangelets crust ($\sim$ 1 year) are two orders of magnitude smaller than quark stars with BPS crust. We can also obtain a direct relation between the relaxation time of quark stars and their gravitational masses (much like that obtained for ordinary stars (Sales et al., 2020)), which is shown in Figure 4.6. We observe that the relaxation time exhibits a linear behavior for both models, with the slope of the curve being more or less inclined depending on the average thickness of the crust in each model.

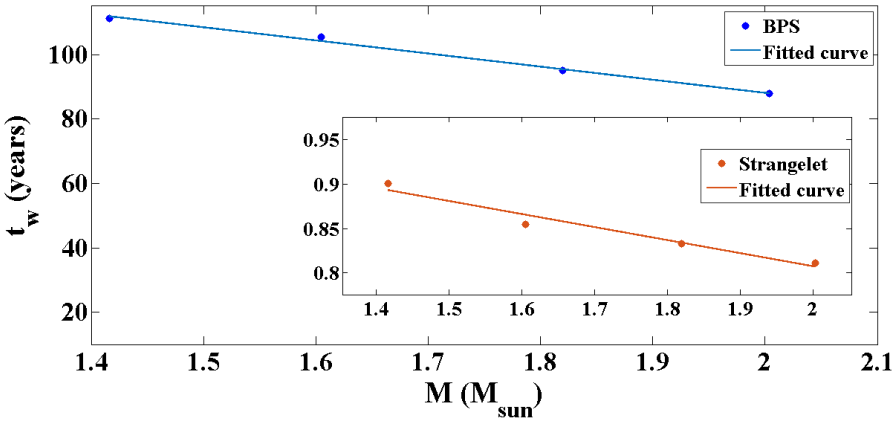


Figure 4.6: Relaxation time vs gravitational mass. The blue line is for quark stars BPS crusted, and the red line is for strangelets crusted. The two models have the same linear behavior, even though the gravitational mass increases while the relaxation time decreases.

### 4.3.5 Superfluidity Effects

In this section, we consider the possibility of color superconductivity. The pattern that will be considered is the Color-Flavor-Locked (CFL) phase (Alford, 2001), where all quarks of all colors are paired to form Cooper pairs at densities of $> 2\epsilon_0$ ($\epsilon_0$ is the nuclear matter density) (Alford et al., 2008). It should be noted that one expects corrections to the quark matter EOS when pairing is present, however, the effects of such corrections to the structure of the star are only noticeable for pairing gaps $\Delta \geq 50$ MeV (Alford and Reddy, 2003). Therefore, for the values of $\Delta$ considered here ($0.1 - 10$ MeV) they can be safely ignored.

Because of pairing, quark stars in the CFL phase will have its neutrino emissions from the direct Urca, the modified Urca and Bremsstrahlung processes suppressed at temperatures $T \leq T_c$, where $T_c$ is the pairing critical temperature (Alford, 2001; Alford et al., 2008). The suppression is due to the pairing of the quarks, and it is given by

$$\epsilon_{DU} \rightarrow \epsilon_{DU} e^{-\Delta/(K_B T)}, \tag{4.28}$$

$$\epsilon_{MU} \rightarrow \epsilon_{MU} e^{-2\Delta/(K_B T)}, \tag{4.29}$$

$$\epsilon_{BR} \rightarrow \epsilon_{BR} e^{-2\Delta/(K_B T)}. \tag{4.30}$$

Where $\Delta$ is the gap parameter for the CFL phase (Alford, 2001; Rajagopal and Wilczek, 2001a,b), and $k_B$ is the Boltzmann constant. Moreover, the specific heat of quark matter is also modified according to

$$C_v^{CFL} = 3.2 C_v \left(\frac{T_c}{T}\right) \left[2.5 - 1.7\left(\frac{T_c}{T}\right) + 3.6\left(\frac{T_c}{T}\right)^2\right] e^{-\Delta/(K_B T)}. \tag{4.31}$$

$T_c$ is the critical temperature below which the phase transition to the CFL state takes place. Currently, $T_c$ is not known, however, it is believed to be smaller than the standard Bardeen-Cooper-Schrieffer ($T_c \approx 0.57\Delta$) (Blaschke et al., 2000). Here, we use $T_c \simeq 0.4\Delta$.

In Figures 4.7- 4.8 we have plotted the cooling curve for quark stars whose quark core is composed of strange quark matter in the CFL state, for different values of gap ($\Delta$) and, we also compare them with stars without superfluidity. In that figures, the quarks stars have masses of $\sim 1.4M$ and $\sim 2.0M$ , respectively. We limit our study to pairing with small gaps, given by $\Delta = 0.1, 1.0, 10$ MeV. We have not considered the cooling from processes involving the Goldstones bosons in the CFL phase. Although these processes are important for the core, they are not effective at cooling stars with a crust, and thermal relaxation of the crust is still the key factor. We note a very distinctive behavior, depending on the value chosen for the superconductivity gap. We see that objects with a higher $\Delta$ (stronger pairing) will result in slower cooling. For completeness, we have also studied scenarios en which $\Delta \geq 10$ MeV and have found that the resulting thermal evolution is essentially the same $\Delta = 10$ MeV. This comes from the fact that the exponential factor $e^{-\Delta/(K_B T)}$ effectively saturates for $\Delta \geq 10$ MeV.

At this point, we would like to observe the following: as the cooling of the core is mainly driven by the exponential suppression of the gap, we believe the value of $T_c$ is not so relevant, so we focused on varying the gap instead. The large value of the CFL gap ($0.1 - 10$ MeV) compared to typical core temperatures implies that the cooling behavior should be relatively insensitive to $T_c$ (Ferrer et al., 2006; Alford et al., 2007; Gerhold and Schäfer, 2006). For the specific heat of the CFL phase, we have used the fitted forms that are simply extensions from nuclear matter. For CFL matter, in principle, one should include the contribution from the (massless) Goldstone boson of the CFL phase. However, such "bare" CFL stars can store a lot of heat and would remain hot for a very

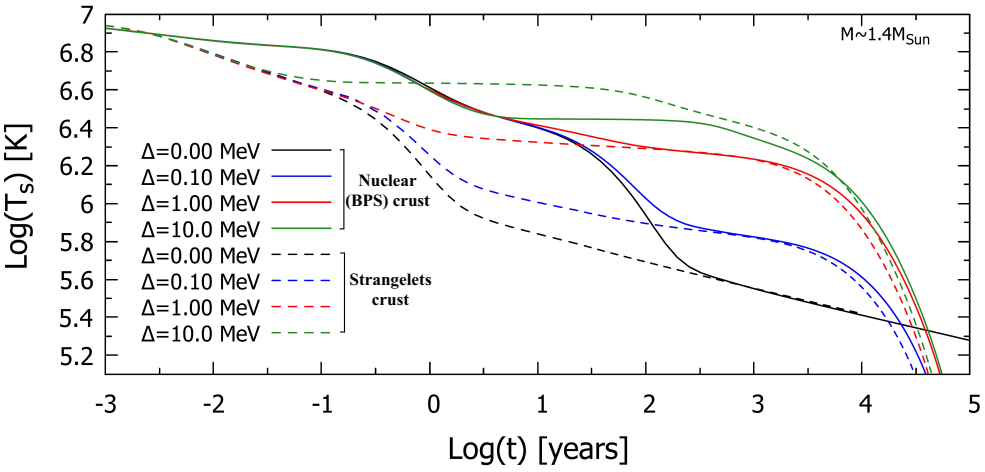


Figure 4.7: Cooling for quark stars with gravitational masses of $\sim 1.4M$ for different values of the CFL gap ($\Delta$). Solid lines represent quark stars with nuclear (BPS) crust, and dashed lines are quark stars with strangelets crust.

long time, in disagreement with the data. Adding a crust allows them to cool, but the large thermal conductivity due to the same bosons basically means that the crust determines the cooling rate. In either case, we return to the same conclusion that the nature of the crust (nuclear or strangelet) plays the main role in cooling strange stars. Also, we note that superconductivity effects were only considered in the quarks at the stellar core. Although there could be pairing in the strangelets, we believe it would not affect the thermal evolution as they have only a passive role - with the electrons dominating the thermal conduction (the strangelets being analogous to the role of ordinary Ions in traditional crust models).

### 4.3.6 Comparison with Observed Data

In this instance, we can use our previous results to compare with the current observations. In Figure 4.9, we compare our theoretical results with a set of observed data as described in Table 4.2 (see Ref. Potekhin et al. (2020)), in which the thermally observable neutron stars are grouped in different classes:

(i) the Weakly magnetized thermal emitters, that include central compact objects and other thermally emitting isolated neutron stars–these mostly emit soft X-ray thermal-like radiation and do not seem to be very strongly

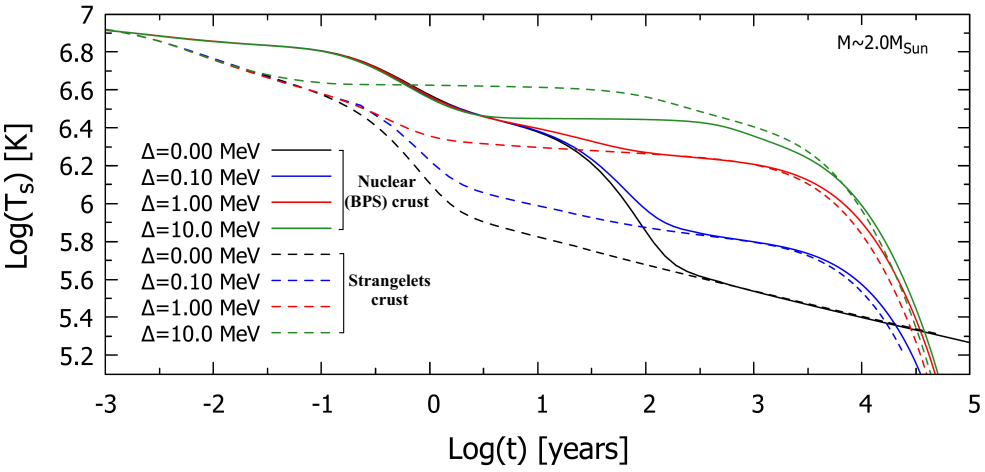


Figure 4.8: Cooling for quark stars with gravitational masses of $\sim 2.0M$ for different values of the CFL gap ($\Delta$). Solid lines represent quark stars with nuclear (BPS) crust, and dashed lines are quark stars with strangelets crust.

magnetized;

(ii) ordinary pulsars, which comprise thermal data associated with rotation powered pulsars with moderate magnetic fields;

(iii) High-B pulsars, objects with strong estimated magnetic fields; and finally

(iv) neutron stars whose temperatures can only be estimated as an upper limit, thought to be associated with relatively young objects (see Potekhin et al. (2020) for more details).

In Fig. 4.9 we show the cooling of $\sim 1.4M$ quark stars –with different pairing gaps– against the observed data described just above. It quickly becomes evident that without pairing the quark, stars cool down too quickly, thus disagreeing with the observed data. Such behavior is not unexpected and has been pointed out in previous works (Negreiros et al., 2012; Alford, 2009). This situation is changed when pairing is included, as the cooling slows down and matches a few of the observed stars. Our results seem to indicate that a moderate pairing with $\Delta \sim 1-10$ MeV is favored if the cooling tracks are to go through the data points.

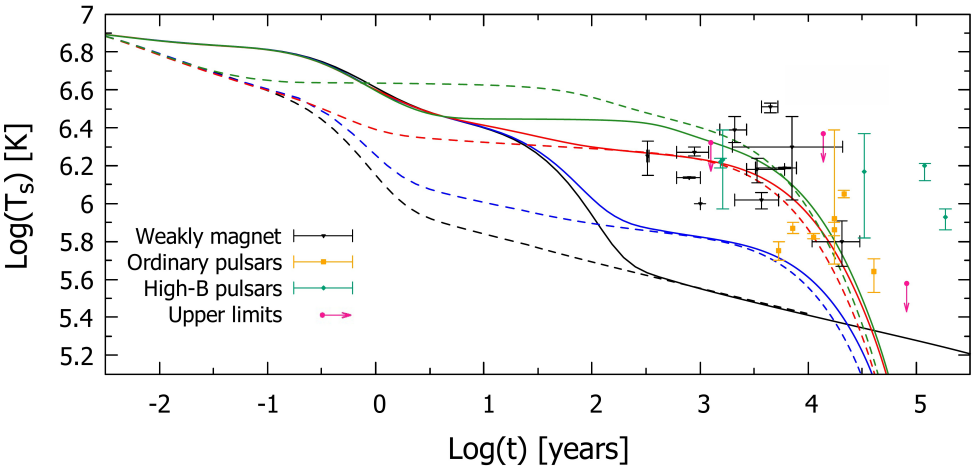


Figure 4.9: Same as Fig. 4.7. The curves are compared with the date from Table 4.2. The data are plotted as indicated in the legend for different neutron stars classes. The error bars show uncertainties.

At this moment, it is opportune to make a few remarks: (i) Fig. 4.9 shows that a large set of the data points (mostly in the ordinary pulsars group) lie to the right of the cooling tracks, indicating old objects. One must note, however, that unless associated with a supernova remnant (not usually the case for ordinary pulsars, with a few exceptions) one can only estimate the NS age by their spin-down[11] properties. Such estimates should be regarded mostly as an upper limit, as the spin-down age is known to be a very crude estimate (in the few cases in which both spin-down and kinematic ages[12] can be estimated simultaneously they vary drastically); (ii) unfortunately the observed data does not help in differentiating between the nuclear and strangelets crusts studies. As explained in the previous section the difference in the crust composition is more strongly manifested in the process of thermalization of the stars, thus, only observation of young stars undergoing such processes (which is not the case with the observed data available) would aid us in differentiating between these models.

[11]Over time, neutron stars slow, as their rotating magnetic fields in effect radiate energy associated with the rotation; older neutron stars may take several seconds for each revolution. This is called spin down. The rate at which a neutron star slows its rotation is usually constant and very small. Spin-down can also be used to calculate the characteristic age of a pulsar.

[12]This is obtained by measuring galactic velocity of the pulsar and tracking it back to the originating supernova remnant

Table 4.2: Age and surface temperature of cooling of some neutron stars, as described in Potekhin et al. (2020). The age is calculated from the expansion rate of the supernova remnant associated with the respective NS, as well as from the transverse velocity of the NS, or by associating the NS with historical supernovae. $K_B T^\infty$ is the surface temperature (in energy units) for a distant observer.

| Short name | Age (Kyr) | $K_B T^\infty$ (eV) |
|---|---|---|
| I. Weakly Magnetized | | |
| 1E 0102 | $2.1 \pm 0.6$ | $240^{+40}_{-30}$ |
| Puppis A NS | $4.45 \pm 0.75$ | $276 \pm 15$ |
| Vela Jr. NS | $2.1 - 5.4$ | $90 \pm 10$ |
| J1046 | $11 - 30$ | $40 - 70$ |
| 1E 1207 | $7^{+14}_{-5}$ | $90 - 250$ |
| J1601 | $0.8 \pm 0.2$ | $118 \pm 1$ |
| J1713 | 1.608 | $138 \pm 1$ |
| J1720 | $0.6 - 1.2$ | $161 \pm 9$ |
| J1732 | $2 - 6$ | $153^{+4}_{-2}$ |
| J1818 | $3.4^{+2.6}_{-0.7}$ | $130 \pm 20$ |
| Kes 79 NS | $6.0^{+1.8}_{-2.8}$ | $133 \pm 1$ |
| Cas A NS | $0.320 - 0.338$ | $123 - 185$ |
| II. Ordinary Pulsars | | |
| J0205 | 5.37 | $49^{+5}_{-6}$ |
| Vela Pulsar | 11.3 | $57^{+3}_{-1}$ |
| J1357 | 7.31 | $64 \pm 4$ |
| B1706 | 17.5 | $71^{+140}_{-30}$ |
| B1823 | 21.4 | $97^{+4}_{-5}$ |
| J2021 | 17.2 | $63^{+6}_{-5}$ |
| B2334 | 40.6 | $38^{+6}_{-9}$ |
| III. High-B pulsars | | |
| J0726 | 186 | $74^{+6}_{-11}$ |
| J1119 | 1.61 | $\sim 80 - 210$ |
| B1509 | 1.56 | $142^{+7}_{-9}$ |
| J1718 | 33.2 | $57 - 200$ |
| J1819 | 120 | $138^{+3}_{-25}$ |
| IV. Upper limits | | |
| J0007 | 13.9 | $< 200$ |
| Crab pulsar | 1.26 | $< 180$ |
| B1727 | 80.5 | $< 30$ |
| J2043 | $1.20 \times 10^3$ | $< 80$ |
| Guitar pulsar | $1.13 \times 10^3$ | $< 110$ |

## 4.4 Summary

In this chapter, we have studied the structure and cooling behavior of quark stars with two different crust models: nuclear (BPS) matter and, strangelets crust. Our goal was to identify possible differences in the cooling behavior of each model, as well as to quantify the thermal relaxation properties of those quark stars (Zapata, J. et al., 2022). Quark stars with nuclear crusts were modeled in the traditional manner, assuming a BPS EOS for the crust beginning at neutron drip density, while for strangelets crusts we followed the foundations laid in reference Alford and Eby (2008); Jaikumar et al. (2006); Alford et al. (2006), i.e., we consider the possibility that the surface tension of quark matter is low enough to allow for the formation of strangelets. Under this hypothesis, it would be energetically favorable for the quark mater at the low densities of a quark star to rearrange itself into a lattice–akin to the manner in which the nuclei organize themselves in the traditional crust model for neutron stars. As shown in Jaikumar et al. (2006) strangelets crust tend to be smaller than their nuclear matter counterpart with spatial extent $\sim$ 20 m, while a nuclear matter crust has a thickness $\sim 0.5$ km. Furthermore, according to Jaikumar et al. (2006), the small mean free path for electrons scattering off nuggets implies that the thermal conductivity in the crust is much smaller than in the core, and they pointed out that the thermal conductivity of strangelets crusts to be similar to that of nuclear crusts. This will influence thermal revolution since the crust will act as an insulator, effectively keeping the surface temperature low (Jaikumar et al., 2006; Gnedin et al., 2001). Given such differences, we sought to quantify how they manifest themselves in a thermal evolution context. Our results indicate that most of the thermal differences between the two models studied are manifested in the initial years of cooling. We have found that quark stars with nuclear (and thus thicker) crusts display a slower cooling behavior when compared with QS with strangelets (thinner crusts). Our assessment is that such behavior is mostly due to the difference in crust thicknesses, as the crust acts mostly as a blanket for the initial years of thermal evolution (Lattimer et al., 1994; Sales et al., 2020; Gnedin et al., 2001). We have also found that the fact that the crust of the QS's studied is populated with strangelets (as opposed to the traditional ions), does not seem to affect the cooling in any major manner. The reason is that as is the case for the ions in regular NS, the strangelets are mostly inert in the context of thermal processes, with the free electrons being the major agents of

heat conduction. In order to quantify our findings, we investigated the thermal relaxation time of quark stars under both models studied, that is, the typical instant when the cold wave reaches the surface of the star. Following the study of Sales et al. (2020), we have found that the star's relaxation time is linearly dependent on the gravitational mass–with a more sloped curve for the QS with strangelets crust (thus indicating a faster relaxation time). Overall we have found that QS with strangelets crust thermalize in $\sim$ 1 year whereas QS with ordinary crust do it in $\sim$ 100 years. We have found that this is mostly due to the fact that strangelet crusts are significantly thinner than ordinary hadronic ones. The different mass of the strangelets (in comparison to ordinary nuclei that compose the crust, also affect the specific heat in the region, although this does not seem to affect the thermal evolution in any major way.

Chapter 5

# Conclusions

The purpose of this thesis was to explore the strangelets manifestation in astrophysical environments. We have focused on two particular objects: strangelet crystal planets (Zapata and Negreiros, 2020), and strange quark stars with strangelets crusts (Zapata, J. et al., 2022). We have adopted the theoretical strange quark matter hypothesis (Bodmer, 1971; Witten, 1984; Terazawa, 1979), in which matter composed of up, down, and strange quarks could be absolutely stable. In this context, we have followed the foundations laid in references Alcock et al. (1986); Heiselberg (1993); Alford et al. (2012); Jaikumar et al. (2006); Alford and Eby (2008) to compute such objects. Thus, our conclusions are:

Firstly, We begin by studying the foundations of this thesis in chapter 2, that is, the strange quark matter (SQM) hypothesis, strangelets and their mass formula, the possibility to have a strangelets crusts on quarks stars' surfaces, and the strange quark matter equation of state in the context of MIT bag model. According to the SQM hypothesis (Bodmer, 1971; Witten, 1984; Terazawa, 1979), matter consisting by up, down and strange quarks have energy per baryon lower than nuclear matter (see estimations in section 2.2). If this were true, there is the possibility that there are nuggets (dimensions of a few Fermis) of strange quark matter called strangelets, and large (dimensions $\sim$ km) compact objects made entirely of such matter called strange quark stars. Here, we have focused on these two possibilities: strangelets and strange quark stars. Strangelets have been investigated in Farhi and Jaffe (1984); Berger and Jaffe (1987); Heiselberg (1993), particularly, Heiselberg (1993) found the correct strangelets mass formula taken into account the screening effects (see section 2.3) inside strangelets. Following this latter work, we have calculated the strangelet masses, $E(Z, A)$, in table 2.3, which change very little for different constant surface tension values $\sigma$. On the other hand, Jaikumar et al. (2006) explored the possibility of the existence of a

strangelets crust on the surfaces of quark stars under certain conditions. They proposed the possibility that the quark stars' crust would consist of strangelets embedded in a uniform electron background. This strangelets crust would behave similarly to the mixed–phase of nuclei and electrons in the crust of ordinary neutron stars. We have adopted this in section 2.4. Finally, in section 2.5, we have explored the strange quark matter equation of state, which is fundamental to determine the stars' properties. We have used the MIT bag model to describe strange quark matter and first order corrections in the strong interaction coupling constant.

In chapter 3, we have started studying the possibility of strangelets are organized in a crystalline structure inside planet-like objects. We have called them strangelet crystal planets (Zapata and Negreiros, 2020). We have followed the ideas from Heiselberg (1993) and Alford et al. (2012) for computing strangelet crystal planets (SCP). Besides, we have investigated the relevant orbital properties associated with these planet-like objects following the references Huang and Yu (2017); Geng et al. (2015). We found in table 3.3.2 that strangelet crystal planets have masses remind us objects like ordinary planets (or sub-stellar objects), but with slightly smaller radii than ordinary planets. Furthermore, we have calculated possible observable signatures of such a model using the concept of tidal disruption radius and amplitude of gravitational waves that could be emitted by such systems. We have found that due to their compactness, the tidal disruption radii of strangelet crystal planets are significantly smaller than those of ordinary planets, however, when compared to previously proposed strange planet models, our scenario leads to higher tidal disruption radii. In addition, ordinary planets have a much lower strain amplitudes than the other SQM objects whereas, strangelet crystal planets and strange planets have the strain amplitude in the same order which could potentially be detected by the future Einstein Telescope or the Advanced LIGO Geng et al. (2015), providing, if detected, evidence for SQM in the form of a strange solar system. Therefore, strangelet crystal planets exhibit intermediate behavior with possible orbital properties not as extreme as those of strange planets (already proposed) but not as mild as those of ordinary planets.

Our assumptions for the existence of strangelet crystal planets are based on the following possible scenarios: first, after the birth of strange quark stars (hot and highly turbulent environment), they may eject low-mass quark nuggets. It

has been suggested that ejection of planetary clumps may happen simultaneously due to the strong turbulence of the strange star surface (Horvath, 2012; Ren-Xin and Fei, 2003). Thus, the strange planetary system can form directly. Second, the contamination processes during the supernova explosion that give birth to a strange star, if the planets of the progenitor star can survive the violent process, may be contaminated by the abundant strange nuggets ejected from the new strange star and then converted to strange planets (Geng et al., 2015; Wolszczan and Frail, 1992). If these planets are remnants of the progenitor star, then there is a possibility that they can be strange planets (Madsen, 1999; Kettner et al., 1995; Caldwell and Friedman, 1991). Third, stellar and planetary strange matter objects could be a remnant of a quark phase in the primordial universe, which may have survived until now (Cottingham et al., 1994); such objects could be very numerous, and they can be captured by strange stars (or neutron stars) to form planetary systems (Chandra and Goyal, 2000). Finally, it was suggested in Caldwell and Friedman (1991) that a high enough cosmic-ray flux of strangelets, produced by strange star mergers, would imply that all neutron stars should be strange stars, as they would have been contaminated by the influx of strangelets.

We intend to pursue further the idea of strangelet crystal planets by adding further sophistication to the model, like a better description of curvature and surface tension effects, exploring their transport and thermal properties, and studying their seismic properties. We are currently investigating the effects of different values for the bag constant on the properties of these objects; this would allow us to investigate the small strangelet flux scenario, as discussed in Bauswein et al. (2009), in which neutron stars and strange stars could potentially coexist. Nonetheless, we believe that the idea set forth in this work introduces interesting possibilities to the already rich study of strange planets and their possible observable signatures (Zapata and Negreiros, 2020). Finally, it is interesting to know how many GW bursts from strange planetary systems could be observed by future GW telescopes each year. It was estimated that the number of strange planetary systems in our Galaxy could be $\sim 10^6$ (Geng et al., 2015), and the timescale for a single planetary system to undergo a collision is $\sim 10^5$ yr. Thus, we estimate that $\sim 10^6/10^5 = 10$ coalescence events could be detected as GW bursts by the future Einstein Telescope (see Geng et al. (2015)).

In chapter 4, we have analyzed the properties of strange quark stars (QS),

that is, their structures and their cooling behavior as well as to quantify the thermal relaxation of those QS. Strange quark stars are structured of a quark matter core and crusted by matter. We have adopted two kinds of crust: a crust made of purely nuclear matter following the BPS equation of state (Baym et al., 1971) and a crust made of strangelets from Jaikumar et al. (2006). Both model have the same quark matter core according to the MIT bag model equation of state. Our goal was to identify possible differences in the cooling behavior of each model, as well as to quantify the thermal relaxation properties of QS. As shown by Jaikumar et al. (2006) strangelet crusts tend to be smaller than their nuclear matter counterpart with spatial extent $\sim 20$ m, while a nuclear matter crust has a thickness $\sim 0.5$ km. Given such differences, we sought to quantify how they manifest themselves in a thermal evolution context (Zapata, J. et al., 2022).

Our results indicate that most of the thermal differences between the two models studied are manifested in the initial years of cooling. Hence, quark stars with nuclear (and thus thicker) crusts display a slower cooling behavior when compared with QS with strangelets (thinner crusts). Our assessment is that such behavior is mostly due to the difference in crust thicknesses, as the crust acts mostly as a blanket for the initial years of thermal evolution (Lattimer et al., 1994; Gnedin et al., 2001; Sales et al., 2020). We have also found that the fact that the crust of the QS's studied is populated with strangelets (as opposed to the traditional ions), does not seem to affect the cooling in any major manner. The reason is that as is the case for the ions in regular NS, the strangelets are mostly inert in the context of thermal processes, with the free electrons being the major agents of heat conduction. In order to quantify our findings, we investigated the thermal relaxation time of quark stars under both models studied, that is, the typical instant when the cold wave reaches the surface of the star. Following the study of Sales et al. (2020), we have found that the star's relaxation time is linearly dependent on the gravitational mass - with a more sloped curve for the QS with strangelet crust (thus indicating a faster relaxation time). Overall we have found that QS with strangelet crust thermalize in $\sim 1$ year whereas QS with ordinary crust do it in $\sim 100$ years. We have found that this is mostly due to the fact that strangelet crusts are significantly thinner than ordinary hadronic ones. The different mass of the strangelets (in comparison to ordinary nuclei that compose the crust, also affect the specific heat in the region, although this does not seem to affect the thermal evolution in any major way.

We aimed to investigate the thermal relaxation of quark stars as well as to explore the thermal properties of previously proposed strangelet crust model. We have found that there is a significant decrease in the relaxation time of QS with strangelet crusts (corresponding to a faster thermal evolution). We have also presented the thermal relaxation time of quark stars as a function of their mass, which as far as we know have not been studied before. We currently are expanding this study to consider the effects of rotation and high magnetic field in the structure of the stars we discussed in this research.

Finally, in this thesis, we have used the strange quark matter hypothesis and explored the manifestation of strange matter in astrophysical environments. Under the strange quark matter hypothesis, we have focused on the context of compact objects (quark stars crusted by strangelets) and planets-like objects (strangelets crystal planets). We can argue that the connection between these two objects lies in the behavior of strange matter at different densities. That is, as the density changes, a possible equilibrium sequence of compact objects ranges from massive strange stars (consisting of a core of strange quark matter surrounded by crusts made of strangelets) to planets-like objects (consisting of crystalline structure made of strangelets). We also have provided some methods to test the strange quark matter in the astrophysical environment, such as tidal disruption radius, orbital period, and gravitational waves signal from the possible existence of strangelet crystal planets. Additionally, thermal behavior and relaxation times from possible existence of strange quarks crusted by strangelets. In Chapter 3, we used strangelets with large $A$ values to develop strangelets crystal planets. Hence, future works can be developed from the following question: What kind of objects would have for strangelets with small $A$ . 100? We think that if we consider strangelets with $A$ small, the result would be white dwarf-like objects. Thus, we would have a complete equilibrium sequence of compact objects. However, in this case, it is necessary to study the behavior of strangelets with small $A$, their mass formula, and so on. Then, we could explore the range of white dwarf densities obtaining white dwarf-like objects and compare them with the ordinary white dwarf stars.

# Bibliography

Abbott, B., Jawahar, S., Lockerbie, N., and Tokmakov, K. (2016). Ligo scientific collaboration and virgo collaboration (2016) directly comparing gw150914 with numerical solutions of einstein's equations for binary black hole coalescence. physical review d, 94 (6). issn 1550-2368, http://dx. doi. org/10.1103/physrevd. 94.064035. *PHYSICAL REVIEW D Phys Rev D*, 94:064035.

Acernese, F., Amico, P., Alshourbagy, M., Antonucci, F., Aoudia, S., Avino, S., Babusci, D., Ballardin, G., Barone, F., Barsotti, L., et al. (2006). The virgo status. *Classical and Quantum Gravity*, 23(19):S635.

Alcock, C., Farhi, E., and Olinto, A. (1986). Strange stars. *The Astrophysical Journal*, 310:261–272.

Alcock, C. and Olinto, A. (1988). Exotic phases of hadronic matter and their astrophysical application. *Annual Review of Nuclear and Particle Science*, 38(1):161–184.

Alford, M. (2001). Color-superconducting quark matter. *Annual Review of Nuclear and Particle Science*, 51(1):131–160.

Alford, M. and Reddy, S. (2003). Compact stars with color superconducting quark matter. *Physical Review D*, 67(7):074024.

Alford, M. G. (2009). Quark matter in neutron stars. *Nuclear Physics A*, 830(1-4):385c–392c.

Alford, M. G., Braby, M., and Schmitt, A. (2007). Critical temperature for kaon condensation in color-flavor-locked quark matter. *Journal of Physics G: Nuclear and Particle Physics*, 35(2):025002.

Alford, M. G. and Eby, D. A. (2008). Thickness of the strangelet-crystal crust of a strange star. *Physical Review C*, 78(4):045802.

Alford, M. G., Han, S., and Reddy, S. (2012). Strangelet dwarfs. *Journal of Physics G: Nuclear and Particle Physics*, 39(6):065201.

Alford, M. G., Rajagopal, K., Reddy, S., and Steiner, A. W. (2006). Stability of strange star crusts and strangelets. *Physical Review D*, 73(11):114016.

Alford, M. G., Schmitt, A., Rajagopal, K., and Schäfer, T. (2008). Color superconductivity in dense quark matter. *Reviews of Modern Physics*, 80(4):1455.

Antoniadis, J., Freire, P. C., Wex, N., Tauris, T. M., Lynch, R. S., Van Kerkwijk, M. H., Kramer, M., Bassa, C., Dhillon, V. S., Driebe, T., et al. (2013). A massive pulsar in a compact relativistic binary. *Science*, 340(6131):1233232.

Armstrong, D. J., de Mooij, E., Barstow, J., Osborn, H. P., Blake, J., and Saniee, N. F. (2016). Variability in the atmosphere of the hot giant planet hat-p-7 b. *Nature Astronomy*, 1(1):1–7.

Auddy, S., Basu, S., and Valluri, S. (2016). Analytic models of brown dwarfs and the substellar mass limit. *Advances in Astronomy*, 2016.

Basri, G. and Brown, M. E. (2006). Planetesimals to brown dwarfs: What is a planet? *Annu. Rev. Earth Planet. Sci.*, 34:193–216.

Bauswein, A., Janka, H.-T., Oechslin, R., Pagliara, G., Sagert, I., Schaffner-Bielich, J., Hohle, M., and Neuhäuser, R. (2009). Mass ejection by strange star mergers and observational implications. *Physical Review Letters*, 103(1):011101.

Baym, G. and Chin, S. (1976). Can a neutron star be a giant mit bag? *Physics Letters B*, 62(2):241–244.

Baym, G., Pethick, C., and Sutherland, P. (1971). The ground state of matter at high densities: equation of state and stellar models. *The Astrophysical Journal*, 170:299.

Berger, M. and Jaffe, R. (1991). Erratum: Radioactivity in strange quark matter. *Physical Review C*, 44(1):566.

Berger, M. S. and Jaffe, R. L. (1987). Radioactivity in strange quark matter. *Physical Review C*, 35(1):213.

Blaschke, D., Klähn, T., and Voskresensky, D. (2000). Diquark condensates and compact star cooling. *The Astrophysical Journal*, 533(1):406.

Bodmer, A. (1971). Collapsed nuclei. *Physical Review D*, 4(6):1601.

Borucki, W. J. (2016). Kepler mission: development and overview. *Reports on Progress in Physics*, 79(3):036901.

Brown, M. E. and Schaller, E. L. (2007). The mass of dwarf planet eris. *Science*, 316(5831):1585–1585.

Buballa, M. (2005). Njl-model analysis of dense quark matter. *Physics Reports*, 407(4-6):205–376.

Burgasser, A. J. (2009). The brown dwarf-exoplanet connection. *arXiv preprint arXiv:0903.1390*.

Burrows, A. and Liebert, J. (1993). The science of brown dwarfs. *Reviews of Modern Physics*, 65(2):301.

Caldwell, R. and Friedman, J. L. (1991). Evidence against a strange ground state for baryons. *Physics Letters B*, 264(1-2):143–148.

Chabrier, G. and Baraffe, I. (2000). Theory of low-mass stars and substellar objects. *Annual Review of Astronomy and Astrophysics*, 38(1):337–377.

Chandra, D. and Goyal, A. (2000). Dynamical evolution of the universe in the quark-hadron phase transition and nugget formation. *Physical Review D*, 62(6):063505.

Chodos, A., Jaffe, R., Johnson, K., and Thorn, C. B. (1974a). Baryon structure in the bag theory. *Physical Review D*, 10(8):2599.

Chodos, A., Jaffe, R., Johnson, K., Thorn, C. B., and Weisskopf, V. (1974b). New extended model of hadrons. *Physical Review D*, 9(12):3471.

Cottingham, W., Kalafatis, D., and Mau, R. V. (1994). Brown dwarfs, quark stars, and quark-hadron phase transition. *Physical review letters*, 73(10):1328.

Demorest, P., Pennucci, T., Ransom, S., Roberts, M., and Hessels, J. (2010). Shapiro delay measurement of a two solar mass neutron star. *arXiv preprint arXiv:1010.5788*.

Farhi, E. and Jaffe, R. L. (1984). Strange matter. *Physical Review D*, 30(11):2379.

Ferrer, E. J., de la Incera, V., and Manuel, C. (2006). Color-superconducting gap in the presence of a magnetic field. *Nuclear Physics B*, 747(1-2):88–112.

Fraga, E. S., Kurkela, A., and Vuorinen, A. (2014). Interacting quark matter equation of state for compact stars. *The Astrophysical Journal Letters*, 781(2):L25.

Friedman, J. L., Ipser, J. R., and Parker, L. (1989). Implications of a half-millisecond pulsar. *Physical review letters*, 62(26):3015.

Frieman, J. A. and Olinto, A. V. (1989). Is the sub-millisecond pulsar strange? *Nature*, 341(6243):633–635.

Fukushima, K. (2003). Relation between the polyakov loop and the chiral order parameter at strong coupling. *Physical Review D*, 68(4):045004.

Fukushima, K. (2004). Chiral effective model with the polyakov loop. *Physics Letters B*, 591(3-4):277–284.

Geng, J., Huang, Y., and Lu, T. (2015). Coalescence of strange-quark planets with strange stars: a new kind of source for gravitational wave bursts. *The Astrophysical Journal*, 804(1):21.

Gerhold, A. and Schäfer, T. (2006). Meson current in the color-flavor-locked phase. *Physical Review D*, 73(12):125022.

Glendenning, N., Kettner, C., and Weber, F. (1995). Possible new class of dense white dwarfs. *Physical review letters*, 74(18):3519.

Glendenning, N. and Weber, F. (1992). Nuclear solid crust on rotating strange quark stars. *Astrophysical Journal*, 400.

Glendenning, N. K. (2012). *Compact stars: Nuclear physics, particle physics and general relativity*. Springer Science & Business Media.

Gnedin, O. Y., Yakovlev, D. G., and Potekhin, A. Y. (2001). Thermal relaxation in young neutron stars. *Monthly Notices of the Royal Astronomical Society*, 324(3):725–736.

Grigorian, H., Blaschke, D., and Voskresensky, D. (2005). Cooling of neutron stars with color superconducting quark cores. *Physical Review C*, 71(4):045801.

Gu, P.-G., Lin, D. N., and Bodenheimer, P. H. (2003). The effect of tidal inflation instability on the mass and dynamical evolution of extrasolar planets with ultrashort periods. *The Astrophysical Journal*, 588(1):509.

Haensel, P. (1991). Transport properties of strange matter. *Nuclear Physics B-Proceedings Supplements*, 24(2):23–28.

Haensel, P., Zdunik, J., and Schaefer, R. (1986a). Strange quark stars. *Astronomy and astrophysics*, 160:121–128.

Haensel, P., Zdunik, J., and Schaeffer, R. (1986b). Changes in stellar parameters implied by a neutron star corequake. *Astronomy and Astrophysics*, 160:251–258.

Heiselberg, H. (1993). Screening in quark droplets. *Physical Review D*, 48(3):1418.

Heiselberg, H., Pethick, C. J., and Staubo, E. (1993). Quark matter droplets in neutron stars. *Physical Review Letters*, 70(10):1355.

Hild, S., Chelkowski, S., and Freise, A. (2008). Pushing towards the et sensitivity using'conventional'technology. *arXiv preprint arXiv:0810.0604*.

Hills, J. (1975). Possible power source of seyfert galaxies and qsos. *Nature*, 254(5498):295–298.

Horvath, J. (2012). The nature of the companion of psr j1719-1438: a white dwarf or an exotic object? *Research in Astronomy and Astrophysics*, 12(7):813.

Huang, Y. and Lu, T. (1997). Strange stars: how dense can their crust be? *Astronomy and Astrophysics*, 325:189–194.

Huang, Y. and Yu, Y. (2017). Searching for strange quark matter objects in exoplanets. *The Astrophysical Journal*, 848(2):115.

Iwamoto, N. (1982). Neutrino emissivities and mean free paths of degenerate quark matter. *Annals of Physics*, 141(1):1–49.

Jaikumar, P., Reddy, S., and Steiner, A. W. (2006). Strange star surface: a crust with nuggets. *Physical review letters*, 96(4):041101.

Jaranowski, P., Krolak, A., and Schutz, B. F. (1998). Data analysis of gravitational-wave signals from spinning neutron stars: The signal and its detection. *Physical Review D*, 58(6):063001.

Kaminker, A., Pethick, C., Potekhin, A., Thorsson, V., and Yakovlev, D. (1998). Neutrino-pair bremsstrahlung by electrons in neutron star crusts. *arXiv preprint astro-ph/9812447*.

Kettner, C., Weber, F., Weigel, M., and Glendenning, N. (1995). Structure and stability of strange and charm stars at finite temperatures. *Physical Review D*, 51(4):1440.

Kurkela, A., Romatschke, P., and Vuorinen, A. (2010). Cold quark matter. *Physical Review D*, 81(10):105021.

Lai, X.-Y. and Xu, R.-X. (2009). Lennard-jones quark matter and massive quark stars. *Monthly Notices of the Royal Astronomical Society: Letters*, 398(1):L31–L35.

Lattimer, J. M., van Riper, K. A., Prakash, M., and Prakash, M. (1994). Rapid cooling and the structure of neutron stars. *The Astrophysical Journal*, 425:802–813.

Li, A., Xu, R.-X., and Lu, J.-F. (2010). Strange stars with different quark mass scalings. *Monthly Notices of the Royal Astronomical Society*, 402(4):2715–2719.

Ma, Z., Dai, Z., Huang, Y., and Lu, T. (2002). The crust properties and cooling of strange stars. *Astrophysics and space science*, 282(3):537–550.

Madsen, J. (1993). Curvature contribution to the mass of strangelets. *Physical review letters*, 70(4):391.

Madsen, J. (1998). How to identify a strange star. *Physical Review Letters*, 81(16):3311.

Madsen, J. (1999). Physics and astrophysics of strange quark matter. In *Hadrons in dense matter and hadrosynthesis*, pages 162–203. Springer.

Miller, M., Lamb, F. K., Dittmann, A., Bogdanov, S., Arzoumanian, Z., Gendreau, K. C., Guillot, S., Harding, A., Ho, W., Lattimer, J., et al. (2019). Psr j0030+ 0451 mass and radius from nicer data and implications for the properties of neutron star matter. *The Astrophysical Journal Letters*, 887(1):L24.

Nambu, Y. and Jona-Lasinio, G. (1961a). Dynamical model of elementary particles based on an analogy with superconductivity. i. *Physical review*, 122(1):345.

Nambu, Y. and Jona-Lasinio, G. (1961b). Dynamical model of elementary particles based on an analogy with superconductivity. ii. *Physical review*, 124(1):246.

Negreiros, R., Dexheimer, V., and Schramm, S. (2012). Quark core impact on hybrid star cooling. *Physical Review C*, 85(3):035805.

Negreiros, R. P. (2009). *Numerical study of the properties of compact stars*. PhD thesis, The Claremont Graduate University and San Diego State University.

Oppenheimer, J. R. and Volkoff, G. M. (1939). On massive neutron cores. *Physical Review*, 55(4):374.

Page, D. and Applegate, J. H. (1992). The cooling of neutron stars by the direct urca process. *The Astrophysical Journal*, 394:L17–L20.

Page, D., Geppert, U., and Weber, F. (2006). The cooling of compact stars. *Nuclear Physics A*, 777:497–530.

Peng, G.-X., Wen, X.-J., and Chen, Y.-D. (2006). New solutions for the color–flavor locked strangelets. *Physics Letters B*, 633(2-3):314–318.

Perryman, M. A. (2000). Extra-solar planets. *Reports on Progress in Physics*, 63(8):1209.

Pizzochero, P. M. (1991). Cooling of a strange star with crust. *Physical review letters*, 66(19):2425.

Potekhin, A., Zyuzin, D., Yakovlev, D., Beznogov, M., and Shibanov, Y. A. (2020). Thermal luminosities of cooling neutron stars. *Monthly Notices of the Royal Astronomical Society*, 496(4):5052–5071.

Potekhin, A. Y., Baiko, D., Haensel, P., and Yakovlev, D. G. (1999). Transport properties of degenerate electrons in neutron star envelopes and white dwarf cores. *arXiv preprint astro-ph/9903127*.

Punturo, M., Abernathy, M., Acernese, F., Allen, B., Andersson, N., Arun, K., Barone, F., Barr, B., Barsuglia, M., Beker, M., et al. (2010). The third generation of gravitational wave observatories and their science reach. *Classical and Quantum Gravity*, 27(8):084007.

Rajagopal, K. and Wilczek, F. (2001a). The condensed matter physics of qcd. In *At The Frontier of Particle Physics: Handbook of QCD (In 3 Volumes)*, pages 2061–2151. World Scientific.

Rajagopal, K. and Wilczek, F. (2001b). Enforced electrical neutrality of the color-flavor locked phase. *Physical Review Letters*, 86(16):3492.

Ratti, C., Thaler, M. A., and Weise, W. (2006). Phases of qcd: Lattice thermodynamics and a field theoretical model. *Physical Review D*, 73(1):014019.

Ren-Xin, X. and Fei, W. (2003). Ultra high energy cosmic rays: Strangelets? *Chinese physics letters*, 20(6):806.

Riley, T. E., Watts, A. L., Bogdanov, S., Ray, P. S., Ludlam, R. M., Guillot, S., Arzoumanian, Z., Baker, C. L., Bilous, A. V., Chakrabarty, D., et al. (2019). A nicer view of psr j0030+ 0451: Millisecond pulsar parameter estimation. *The Astrophysical Journal Letters*, 887(1):L21.

Sales, T., Lourenço, O., Dutra, M., and Negreiros, R. (2020). Revisiting the thermal relaxation of neutron stars. *Astronomy & Astrophysics*, 642:A42.

Sarma, R., Baruah, K., and Sarma, J. (2008). Iau planet definition: Some confusions and their modifications. *arXiv preprint arXiv:0810.0993*.

Schneider, J., Dedieu, C., Le Sidaner, P., Savalle, R., and Zolotukhin, I. (2011). Defining and cataloging exoplanets: the exoplanet. eu database. *Astronomy & Astrophysics*, 532:A79.

Shapiro, S. L. and Teukolsky, S. A. (2008). *Black holes, white dwarfs, and neutron stars: The physics of compact objects*. John Wiley & Sons.

Shibata, M., Zhou, E., Kiuchi, K., and Fujibayashi, S. (2019). Constraint on the maximum mass of neutron stars using gw170817 event. *Physical Review D*, 100(2):023015.

Shohet, J. (2003). Plasma science and engineering. In Meyers, R. A., editor, *Encyclopedia of Physical Science and Technology (Third Edition)*, pages 401–423. Academic Press, New York, third edition edition.

Stejner, M. and Madsen, J. (2005). Gaps below strange star crusts. *Physical Review D*, 72(12):123005.

Terazawa, H. (1979). Ins-report, 336 (ins, univ. of tokyo); 1989. *J. Phys. Soc. Japan*, 58(3555):1989.

Thorne, K. S. (1977). The relativistic equations of stellar structure and evolution. *The Astrophysical Journal*, 212:825–831.

Tolman, R. C. (1939). Static solutions of einstein's field equations for spheres of fluid. *Physical Review*, 55(4):364.

Tsuruta, S. (1998). Thermal properties and detectability of neutron stars. ii. thermal evolution of rotation-powered neutron stars. *Physics Reports*, 292(1-2):1–130.

Usov, V. V. (1997). Low-mass normal-matter atmospheres of strange stars and their radiation. *The Astrophysical Journal*, 481(2):L107.

Van Riper, K. A. (1991). Neutron star thermal evolution. *The Astrophysical Journal Supplement Series*, 75:449–462.

Weber, F. (2005). Strange quark matter and compact stars. *Progress in Particle and Nuclear Physics*, 54(1):193–288.

Weber, F. (2017). *Pulsars as astrophysical laboratories for nuclear and particle physics*. Routledge.

Weber, F., Negreiros, R., and Rosenfield, P. (2009). Neutron star interiors and the equation of state of superdense matter. In *Neutron Stars and Pulsars*, pages 213–245. Springer.

Weber, F., Schaab, C., Weigel, M., and Glendenning, N. (1996). From quark matter to strange machos. *arXiv preprint astro-ph/9609067*.

Witten, E. (1984). Cosmic separation of phases. *Physical Review D*, 30(2):272.

Wolszczan, A. and Frail, D. A. (1992). A planetary system around the millisecond pulsar psr1257+ 12. *Nature*, 355(6356):145–147.

Yakovlev, D., Kaminker, A., Gnedin, O. Y., and Haensel, P. (2001). Neutrino emission from neutron stars. *Physics Reports*, 354(1-2):1–155.

Zapata, J. and Negreiros, R. (2020). Orbital properties and gravitational-wave signatures of strangelet crystal planets. *The Astrophysical Journal*, 892(1):67.

Zapata, J., Sales, T., Jaikumar, P., and Negreiros, R. (2022). Thermal relaxation and cooling of quark stars with a strangelet crust. *A&A*, 663:A19.

Appendix A

# Physical Constants

The following Table A lists the values of physical constants relevant to this thesis.

Table A.1: Table of physical constants.

| Physical constant | Symbol | Value |
|---|---|---|
| Electron charge | $e$ | $1.602 \times 10^{-19}\ C$ |
| Electron mass | $m_e$ | $9.10938356 \times 10^{-31}\ kg$ |
| Speed of light | $c$ | $2.99792 \times 10^{8}\ m/s$ |
| Planck's constant | ~ | $1.0546 \times 10^{-34}\ J.s$ |
| Boltzmann's constant | $K_B$ | $1.3807 \times 10^{-23}\ J.K^{-1}$ |
| Stefan-Boltzmann's constant | $\sigma_{SB}$ | $5.6697 \times 10^{-8}\ Wm^{-2}K^{-4}$ |
| Bohr radius | $r_{Bohr}$ | $5.29 \times 10^{-11}\ m$ |
| Baryon number density | $\rho_0$ | $0.16\ fm^{-3}$ |
| Density of nuclear matter | $\epsilon_0$ | $2.8 \times 10^{14}\ g/cm^3$ |
| Gravitational constant | $G$ | $6.6726 \times 10^{-11}\ m^3kg^{-1}s^{-2}$ |
| Solar mass | $M$ | $1.99 \times 10^{30}\ kg$ |
| Jupiter's mass | $M_J$ | $10^{-3}M$ |
| Parsec | $pc$ | $3.08568 \times 10^{16}\ m$ |

Appendix B

# Fermi-gas Equation of State for Nucleons and Electrons

Here, we describe the equation of state for nucleons and electrons appropriate for the description of compact objects. Here, we consider an idealized composition of dense matter for compact stars (white dwarfs and neutron stars), that is, a non-interacting neutrons, protons, and electrons gas in such proportions at each baryon number density that the gas has its lowest possible energy (i e., beta equilibrium). Additionally, we must demand that the minimum energy be found subject t the constraint of electrical neutrality. Baryon density is usually employed as an independent variable in calculating an equation of state because baryon number is conserved. We consider a prototype for any more sophisticated model of equation of state of dense charge-neutral matter.

We deal with a degenerate ideal Fermi gas (since neutrons, protons, and electrons are fermions). Ideal in this context means that interactions are ignored. Degenerate means that all quantum states up to a given energy, called the Fermi energy, are occupied. We wish to calculate the equation of state, which is the pressure and energy density at a common value of the density, or alternately, the value of the pressure at a given energy density. Each Fermion type ($n$,$p$,$e$) contributes to the energy density, pressure, and number density according to

Glendenning (2012)

$$\begin{aligned}\epsilon &= \frac{1}{4\pi^2}\left[\mu k\left(\mu^2-\frac{m^2}{2}\right)-\frac{1}{2}m^4 ln\left(\frac{\mu+k}{m}\right)\right],\\ p &= \frac{1}{12\pi^2}\left[\mu k\left(\mu^2-\frac{5m^2}{2}\right)+\frac{3}{2}m^4 ln\left(\frac{\mu+k}{m}\right)\right],\\ \rho &= \frac{k^3}{3\pi^2}\end{aligned} \tag{B.1}$$

where $\mu = (m^2+k^2)^{1/2}$, is the Fermi energy (or the chemical potential), and $k$ the Fermi momentum.

The high-density limit $k >> m$, which may also be called the relativistic limit if $m$ is not ignored, or the ultra-relativistic limit if it can be. The results are Glendenning (2012)

$$\begin{aligned}\epsilon &\approx \frac{1}{4\pi^2}\left[k^4-\frac{1}{2}m^4 ln\left(\frac{2k}{m}\right)\right],\\ p &\approx \frac{1}{12\pi^2}\left[k^4+\frac{3}{2}m^4 ln\left(\frac{2k}{m}\right)\right].\end{aligned} \tag{B.2}$$

The logarithmic terms are small compared to $k^4$ in the ultra-relativistic limit, so we have

$$\epsilon \to 3p \approx \frac{1}{4\pi^2}(3\pi^2\rho)^{4/3} \quad (high\ density, k >> m) \tag{B.3}$$

where $\rho$ is the density of fermion type considered. The very low density, the non-relativistic approximation is:

$$\begin{aligned}\epsilon &\approx \rho m + \frac{(3\pi^2\rho)^{5/3}}{10\pi^2 m},\\ p &\approx \frac{(3\pi^2\rho)^{5/3}}{15\pi^2 m} \quad (low\ density, k << m)\end{aligned} \tag{B.4}$$

It is observed that the term $\epsilon$ proportional to $\rho$ does not contribute to the pressure. These are the contributions of each type of fermion to the equation of state.

Appendix C

# Tolman-Oppenheimer-Volkoff Equations

Here, we proceed to derive the stellar structure equations of a non-rotating, static, spherically symmetric compact star. The metric of such an object has the form Weber (2017)

$$ds^2 = -e^{2\Phi(r)}dt^2 + e^{2\Lambda(r)}dr^2 + r^2 d\Omega^2, \tag{C.1}$$

where $\Phi(r)$ and $\Lambda(r)$ are the radially metric functions and, $d\Omega^2 = d\theta^2 + \sin^2\theta d\phi^2$. Introducing the covariant components of the metric tensor as,

$$g_{tt} = -e^{2\Phi}, g_{rr} = e^{2\Lambda}, g_{\theta\theta} = r^2, g_{\phi\phi} = r^2 sin^2\theta. \tag{C.2}$$

The contravariant components of the metric tensor are obtained via the relation: $g^{\mu\nu}g_{\nu\lambda} = \delta^\mu_\nu$, where $\delta^\mu_\nu$ is the four-dimensional Kronecker delta. So we find

$$g^{tt} = -e^{-2\Phi}, g^{rr} = e^{-\Lambda}, g^{\theta\theta} = r^{-2}, g^{\phi\phi} = \frac{1}{r^2 sin^2\theta} \tag{C.3}$$

Because of the underlying symmetries, the only functional dependence that enters the metric is the dependence on radial distance $r$, measured from the star's origin. We can also find the mixed components of the metric tensor (remembering $g^\mu_\lambda = g^{\mu\nu}g_{\nu\lambda}$, and the metric tensor obey $g^\mu_\lambda = \delta^\mu_\nu$) and therefore: $g^t_t = g^r_r = g^\theta_\theta = g^\phi_\phi = 1$. The determinant of $g_{\mu\nu}$ is from (C.2):

$$g \equiv det(g_{\mu\nu}) = -e^{2\Phi}e^{2\Lambda}r^4 sin^2\theta. \tag{C.4}$$

With these things, we can now proceed to calculate the Einstein tensor associated with the metric (C.2). To do that, we need to find the Riemann tensor $R^{\tau}_{\mu\sigma\nu}$ and the curvature scalar $R$ given in terms of the components of the metric tensor and derivatives thereof. The source of the gravitational field for the static star model consists simply of the matter that makes up the star. Thus, the energy-momentum tensor will be solely related to the properties of the matter that makes up the star.

First, we determine the Christoffel symbols $\Gamma^{\sigma}_{\mu\nu}$. The non-vanishing symbols to the form of line element (C.1) of a spherically symmetric body are,

$$\begin{aligned}
&\Gamma^{r}_{tt} = e^{2\Phi-2\Lambda}\Phi\ , \Gamma^{t}_{tr} = \Phi\ , \Gamma^{r}_{rr} = \Lambda\ , \\
&\Gamma^{\theta}_{r\theta} = r^{-1}, \Gamma^{\phi}_{r\phi} = r^{-1}, \Gamma^{r}_{\theta\theta} = -re^{-2\Lambda}, \Gamma^{\phi}_{\theta\phi} = \frac{cos\theta}{sin\theta} \\
&\Gamma^{r}_{\phi\phi} = -rsin^{2}\theta e^{-2\Lambda}, \Gamma^{\theta}_{\phi\phi} = -sin\theta cos\theta.
\end{aligned} \tag{C.5}$$

Where primes denote differentiation with respect to the radial coordinate $r$, ($\Phi \equiv d\Phi/dr$ and $\Phi \equiv d^{2}\Phi/dr^{2}$). With the Christoffel symbols we calculate of the Riemann tensor $R^{\tau}_{\mu\nu\sigma}$, the Ricci tensor $R_{\mu\nu}$ and the Ricci scalar $R$, respectively, of which the Einstein tensor is composed (see in Weber (2017)). After some algebra, the non-vanishing components of the Riemann tensor:

$$\begin{aligned}
&R^{t}_{rtr} = -\Phi\ \ - (\Phi\ )^{2} + \Phi\ \Lambda\ , \\
&R^{t}_{\theta t\theta} = -r\Phi\ e^{-2\Lambda}, R^{t}_{\phi t\phi} = -r\Phi\ sin^{2}\theta e^{-2\Lambda}, \\
&R^{r}_{ttr} = \{-\Phi\ \ - (\Phi\ )^{2} + \Phi\ \Lambda\ \}e^{2\Phi-2\Lambda}, \\
&R^{r}_{\theta t\theta} = r\Lambda\ e^{-2\Lambda}, R^{r}_{\phi r\phi} = \Lambda\ rsin^{2}\theta r^{-2\Lambda}, \\
&R^{\theta}_{tt\theta} = -\Phi\ re^{2\Phi-2\Lambda}, R^{\theta}_{rr\theta} = -\frac{1}{r}\Lambda\ , \\
&R^{\theta}_{\phi\theta\phi} = sin^{2}\theta(1 - e^{-2\Lambda}), R^{\phi}_{tt\phi} = -\Phi\ re^{2\Phi-2\Lambda}, \\
&R^{\phi}_{rr\phi} = -\frac{1}{r}\Lambda\ , R^{\phi}_{\theta\theta\phi} = -1 + e^{-2\Lambda}.
\end{aligned} \tag{C.6}$$

The components of Ricci tensor are

$$\begin{aligned} R_{tt} &= \{-\Phi\ \Lambda\ + \Phi\ \ + (\Phi\ )^2 + 2r^{-1}\Phi\ \}e^{2\Phi-2\Lambda}, \\ R_{rr} &= -\Phi\ \ - (\Phi\ )^2 + \Phi\ \Lambda\ + \frac{2}{r}\Lambda\ , \\ R_{\theta\theta} &= \{-r\Phi\ + r\Lambda\ + e^{2\Lambda} - 1\}e^{-2\Lambda}, \\ R_{\phi\phi} &= -sin^2\theta\{r\Phi\ - r\Lambda\ - e^{2\Lambda} + 1\}e^{-2\Lambda}, \end{aligned} \tag{C.7}$$

The Ricci scalar has the form

$$R = \{+2\Phi\ \Lambda\ r^2 - 2\Phi\ \ r^2 - 2(\Phi\ )^2 - 4r\Phi\ + 4r\Lambda\ + 2e^{2\Lambda} - 2\}r^{-2}e^{-2\Lambda}. \tag{C.8}$$

The Einstein tensor, $G_{\mu\nu}$, could now be calculated. However, it is more convenient to transform $G_{\mu\nu}$ to its mixed representation $G^{\mu}_{\nu}$, according to the rules $g^{\mu\kappa}G_{\kappa\nu}$ and summing over $\kappa$. Thus, the $G^{\mu}_{\nu}$ tensor in the mixed representation reads

$$G^{\mu}_{\nu} \equiv R^{\mu}_{\nu} - \frac{1}{2}\delta^{\mu}_{\nu}R = 8\pi T^{\mu}_{\nu}. \tag{C.9}$$

with the energy-momentum tensor:

$$T^{\mu}_{\nu} = (\epsilon + P)\frac{dx^{\mu}}{d\tau}\frac{dx_{\nu}}{d\tau} + \delta^{\mu}_{\nu}P. \tag{C.10}$$

where $T^t_t = -\epsilon$ and $T^r_r = T^{\theta}_{\theta} = T^{\phi}_{\phi} = P$.

The components of the Einstein tensor in the mixed representation

$$\begin{aligned} G^t_t &= R^t_t - \frac{1}{2}R = e^{-2\Lambda}\left(\frac{1}{r^2} - 2\frac{\Lambda}{r}\right) - \frac{1}{r^2}, \\ G^r_r &= R^r_r - \frac{1}{2}R = e^{-2\Lambda}\left(2\frac{\Phi}{r} + \frac{1}{r^2}\right) - \frac{1}{r^2}, \\ G^{\theta}_{\theta} &= R^{\theta}_{\theta} - \frac{1}{2}R = e^{-2\lambda}\left(\Phi\ \ - \Phi\ \Lambda\ + (\Phi\ )^2 + \frac{\Phi\ - \Lambda}{r}\right), \end{aligned} \tag{C.11}$$

and $G^{\phi}_{\phi} = G^{\theta}_{\theta}$. We can therefore go back to Einstein's field equations and obtain

the differential equations that determine the metric inside the star:

$$\begin{aligned} e^{-2\Lambda}\left(2\frac{\Lambda}{r}-\frac{1}{r^2}\right)+\frac{1}{r^2} &= 8\pi\epsilon, \\ e^{-2\Lambda}\left(2\frac{\Phi}{r}+\frac{1}{r^2}\right)-\frac{1}{r^2} &= 8\pi P, \\ e^{-2\Lambda}\left(\Phi\ -\Phi\,\Lambda\ +(\Phi\ )^2+\frac{\Phi\ -\Lambda}{r}\right) &= 8\pi P, \end{aligned} \tag{C.12}$$

and $G^{\phi}_{\phi} = G^{\theta}_{\theta}$, and $T^{\phi}_{\phi} = T^{\theta}_{\theta}$. The stellar structure equations in their final form are now readily found as follows. Let us introduce the quantity $m(r)$ as,

$$m(r) \equiv 4\pi \int_0^r dr r^2 \epsilon(r), \rightarrow \frac{dm}{dr} = 4\pi r^2 \epsilon(r). \tag{C.13}$$

which can be interpreted as the amount of mass energy contained in a sphere of radius $r$. At the star's origin, we impose the condition $m(0) = 0$. With this definition, Einstein's field equation (C.12) can be integrated. From the first expression of (C.12), we have

$$e^{-\Lambda} = 1 - \frac{2m}{r}. \tag{C.14}$$

In the next step we add the first two expression from (C.12) which gives

$$8\pi(\epsilon + P) = \frac{2}{r} e^{-2\Lambda}(\Lambda\ +\Phi\ ). \tag{C.15}$$

The metric function $\Lambda$ can be eliminated (using (C.14)) and after some algebraic manipulations ones arrives at

$$8\pi P = -\frac{2m}{r^3} + 2\left(1 - \frac{2m}{r}\right)\frac{\Phi}{r}. \tag{C.16}$$

and then, this expression for $\Phi$ gives

$$\Phi\ = \frac{4\pi r^3 P + m}{r^2(1 - 2m/r)} \tag{C.17}$$

Finally, we arrive for the pressure gradient inside a spherically symmetric configuration

$$\frac{dP}{dr} = -\frac{[\epsilon(r) + p(r)][m(r) + 4\pi r^3 p(r)]}{r(r - 2m(r))} \tag{C.18}$$

With the central pressure $P(r = 0) = P(\epsilon_c)$ and $\epsilon_c$ as the star's central mass

energy density. This final result is known as the Tolman-Oppenheimer-Volkoff (TOV) equation Tolman (1939). This equation is fundamental to the description of the structure of a hydrostatically stable stellar configuration treated in the framework of Einstein's general theory of relativity. As in classical Newtonian mechanics, so also in Einstein's theory. The force that acts on a mass shell inside the star is the pressure force of the stellar matter enclosed in that shell, which acts in the radial outward direction. Gravity pulls on that mass shell in the radial inward direction such that both forces, because of hydrostatic equilibrium, counterbalance each other.

Appendix D

# Stellar Cooling Equations

We present the mathematical model used to describe the thermal evolution of a star. The star is assumed to be a rigid object, so there is no transport of matter. Thus, there is no heat exchange by convection, there is no differential rotation[1], there is no heat from friction. Even a rigid rotation for the star is not assumed, as well as in the calculation of its structure. Therefore, the equations adopted and the quantities involved, such as temperature $T$, will all be spherically symmetric, depending only on the radial position $r$ and the time $t$.

The exchange of energy will take place, finally, only by thermal conduction, inside the star; and irradiation, on its surface. It is also necessary to take into account the amount of energy lost at each position in the interior of the star due to the escape of neutrinos Weber (2017); Thorne (1977); Van Riper (1991). For each location within the star, the expression for the conservation of energy must then have three terms. One that denotes the exchange of heat by conduction between a given location and adjacent regions, a second that represents the amount of energy lost by the escape of neutrinos from that location, and the last one related to the variation of the internal energy, and therefore of the temperature, of the matter at that location.

The amount of energy lost by neutrinos is determined by a quantity known as the neutrino emissivity, $\epsilon_\nu = \epsilon_\epsilon(r, T)$, a function of position $r$ and temperature $T$. The neutrino emissivity is calculated separately from the reaction probability rate of each neutrino-producing process. Thus, before calculating the cooling, the behavior of neutrino emissivity $\epsilon_\nu(r, T)$ is already known. Therefore, this quantity dictates, at each instant, the amount of energy per unit of volume, per

[1]Differential rotation is seen when different parts of a rotating object move with different angular velocities (rates of rotation) at different latitudes and/or depths of the body and/or in time. This indicates that the object is not solid.

unit of time, lost in a given position within the star.

The conservation of energy alone is not, however, sufficient to show how the system evolves, since there are two other terms in it that, in principle, are indeterminate. However, the heat flux by thermal conduction can be determined by the heat transport equation, which relates such flux to a given temperature gradient. The amount of energy that flows from the warmer to the cooler layer depends on the thermal conductivity $\kappa = \kappa(r, T)$ of matter at a given location and temperature. With the determination of the heat flux and the energy lost by the neutrinos, conservation of energy dictates how the temperature will change at a given position. How much the temperature varies depends on the specific heat $c_v$ of that location, for a given value of $T$.

The differential equations that govern, therefore, the thermal evolution of a star are Weber (2017); Thorne (1977); Van Riper (1991)

$$\frac{\partial(l(r,T)e^{2\Phi(r)})}{\partial m} = -\frac{1}{\epsilon(r)\sqrt{1-2m(r)/r}}\times \left(\epsilon_\nu(r,T)e^{2\Phi(r)} + c_v(r,T)\frac{\partial(T(r,T)e^{\Phi(r)})}{\partial t}\right) \tag{D.1}$$

$$\frac{\partial(T(r,T)e^{\Phi(r)})}{\partial m} = -\frac{(l(r,T)e^{\Phi(r)})}{16\pi^2 r^4 \kappa(r,T)\epsilon(r)\sqrt{1-2m(r)/r}}, \tag{D.2}$$

The first is precisely the energy balance equation, or energy conservation, and the second is the heat transport equation. They are, therefore, the luminosity gradient $l = l(r, t)$ and the temperature gradient $T = T(r, t)$, respectively. The luminosity gradient represents the amount of energy that is lost per unit of time from a given layer by thermal conduction. Thus, if we take the difference of the luminosity at a certain position $r + dr$ with the luminosity at $r$ and divide it with the volume ($dV = 4\pi r^2 dr$) of the layer comprised between these two positions, we obtain (in the limit $dr \to 0$), the amount of energy lost per unit volume, per unit time, at a given position within the star:

$$\lim_{dr\to 0}\frac{l(r+dr)-l(r)}{4\pi r^2 dr} = \frac{1}{4\pi r^2}\frac{\partial l}{\partial r} \tag{D.3}$$

Fig. D.1 illustrates what is expressed in Eq. (D.3) The outgoing arrow indicates the position $r$ of a certain layer of thickness $dr$ and volume $dV = 4\pi r^2 dr$, while the incoming arrows indicate the luminosity on spherical surfaces of radius $r$

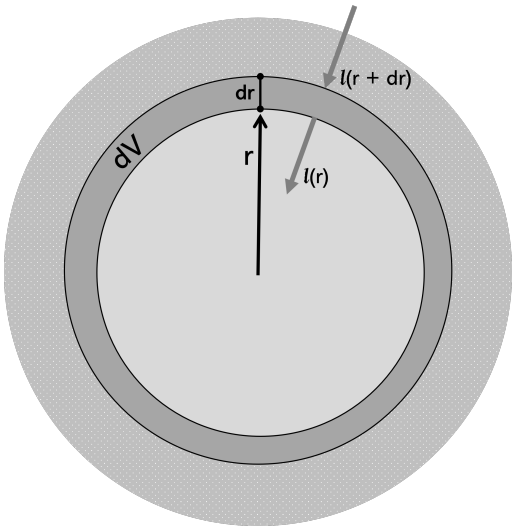


Figure D.1: Illustration of the amount of energy lost in a certain layer of the star.

and $r + dr$ (they point to the center of the star, as in the initial phases of the star's cooling, the luminosity inside the star is negative, that is, heat flows from the most superficial layers towards the center, this is because the intense emissivity of neutrinos in the innermost layers lowers the temperature in these regions, generating a temperature gradient of so that the center is cooler than the outermost layers).

It happens that the star is a very compact object (for example NS and QS), causing its gravitational field to be intense, thus curving the surrounding space-time. This curvature ends up altering the energy flow between the layers due to the *redshift* that energy suffers when crossing the layer and also to the time dilation existing between these two surfaces, causing it to be corrected by the factor $e^{\Phi(r)}$ (see Weber (2017)). Also, because of gravity we must use the proper value of the layer thickness, corrected by the factor $e^{\Lambda(r)}$ (where $e^{2\Phi(r)}$ and $e^{2\Lambda(r)}$ are the temporal component of the metric and the radial component of the metric, respectively).

The amount of energy lost per unit volume, per unit time, $\varepsilon$, through thermal

conduction to a given position $r$, is given by:

$$\begin{aligned}\varepsilon(r) &= \frac{1}{4\pi r^2}\frac{1}{e^{\Lambda(r)}}\frac{\partial(le^{2\Phi(r)})}{\partial r} \\ &= \frac{1}{4\pi r^2}\sqrt{1-\frac{2m(r)}{r}}\frac{\partial(le^{2\Phi(r)})}{\partial r} \\ &= \frac{1}{4\pi r^2}\sqrt{1-\frac{2m(r)}{r}}\frac{dm}{dr}\frac{\partial(le^{2\Phi(r)})}{\partial r} \\ &= \frac{1}{4\pi r^2}\sqrt{1-\frac{2m(r)}{r}}(4\pi r^2\epsilon(r))\frac{\partial(le^{2\Phi(r)})}{\partial r} \\ &= \epsilon(r)\sqrt{1-\frac{2m(r)}{r}}\frac{\partial(le^{2\Phi(r)})}{\partial r}\end{aligned} \tag{D.4}$$

In order to obtain the two other terms in parentheses in Eq. (D.1) consider the amount of energy lost by neutrino emission per unit volume, per unit time; and the rate of change of internal energy per unit volume of matter, denoted, respectively, by $\epsilon_\nu(r,T)$ and $\rho\frac{\partial}{\partial t}\left(\frac{u(r)}{\rho(r)}\right)$, where $u$ and $\rho$ being the internal energy per unit volume and the baryonic number density, respectively. These terms have to be corrected also by the $e^{2\Phi(r)}$ term, in addition to taking the derivative with respect to proper time $\frac{\partial}{\partial\tau} = \frac{1}{e^{\Phi(r)}}\frac{\partial}{\partial t}$. We therefore obtain

$$\begin{aligned}\epsilon_\nu(r,T)\cdot e^{2\Phi(r)}, \\ \frac{\rho(r)}{e^{\Phi(r)}}\frac{\partial}{\partial t}\left(\frac{u(r)}{\rho(r)}\right)\cdot e^{2\Phi(r)}.\end{aligned} \tag{D.5}$$

The second term can be rewritten as:

$$\frac{\rho(r)}{r^{\Phi(r)}}\frac{\partial}{\partial t}\left(\frac{u(r)}{\rho(r)}\right)\cdot e^{2\Phi(r)} = \rho(r)\frac{\partial}{\partial T(r,t)}\left(\frac{u(r)}{\rho(r)}\right)\frac{\partial T(r,t)}{\partial t}\cdot e^{\Phi(r)}, \tag{D.6}$$

such that the derivative with respect to temperature is made at constant volume and baryonic number (there is no expansion or contraction of the layer in question, and the reactions that occur between the particles conserve the baryonic number). The expression $\bar{c}_v = \frac{\partial}{\partial T(r,t)}\left(\frac{u(r)}{\rho(r)}\right)$ is the definition of specific heat at constant volume per particle, which in turn is equal to $c_v/\rho(r)$. Then, the term in (D.6) can therefore be rewritten as:

$$c_v\frac{\partial T(r,t)}{\partial t}\cdot e^{\Phi(r)} = c_c\frac{\partial(T(r,t)e^{\Phi(r)})}{\partial t} \tag{D.7}$$

In order that, for each position $r$, energy is conserved, the amount of energy per unit volume, per unit time, that leaves this position by conduction, plus the energy also per unit volume and time that leaves this position. position, due to neutrino leakage, must be equal to the rate of decrease of the internal energy density:

$$\varepsilon(r)\sqrt{1-\frac{2m(r)}{r}}\frac{\partial(le^{2\Phi(r)})}{\partial m}+\epsilon_\nu(r,T)\cdot e^{2\Phi(r)}=-c_v\frac{\partial(T(r,r)e^{\Phi)(r)}}{\partial t}, \tag{D.8}$$

where we get Eq. (D.1).

Equation (D.2) can be obtained by generalizing the classical theory of heat transport. The expression for the heat flux through a cross-sectional area A is given by:

$$l=-\kappa A\frac{\partial T}{\partial x}. \tag{D.9}$$

For a spherical shell, the cross–section has area $A=4\pi r^2$, with heat propagating in the radial direction $r$. the previous equation becomes:

$$l=-4\pi r^2\kappa\frac{\partial T}{\partial r}. \tag{D.10}$$

Here it is also necessary to make the necessary relativistic corrections (see Weber (2017) for more details). In this way, Eq. (D.10) takes the following form:

$$le^{\Phi}=-4\pi r^2\kappa\sqrt{1-\frac{2m(r)}{r}}\frac{\partial Te^{\Phi}}{\partial r} \tag{D.11}$$

after a little algebra on the previous equation, we get:

$$\begin{aligned} le^{\phi}&=-4\pi r^2\kappa\sqrt{1-\frac{2m(r)}{r}}\frac{dm}{dr}\frac{\partial Te^{\Phi}}{\partial r}\\ le^{\phi}&=-4\pi r^2\kappa\sqrt{1-\frac{2m(r)}{r}}(4\pi r^2\epsilon(r))\frac{\partial Te^{\Phi}}{\partial r}\\ le^{\phi}&=-16\pi^2r^4\kappa\epsilon(r)\sqrt{1-\frac{2m(r)}{r}}\frac{\partial Te^{\Phi}}{\partial r} \end{aligned} \tag{D.12}$$

and, finally, from Eq. (D.12), we obtain Eq. (D.2).

In this research, Eqs. (D.1) and (D.2) were solved numerically. The emissivity of neutrinos $\epsilon_\nu$ is given by an analytical expression, being different in the crust

and in the core of the star. The same is true for the specific heat $c_v$ and the thermal conductivity $\kappa$. However, other quantities present in these equations, as the accumulated gravitational mass m(r) and the energy density $\epsilon(r)$, were previously obtained from the structure equations, and from the equation of a microscopic model from which one obtains the equation of state (EOS) of matter inside the star relating $\epsilon$ and the pressure $p$.